AD/A-004 020

PRELIMINARY INVESTIGATION OF THE DYNAMIC FORCE RESPONSE COEFFICIENTS FOR SQUEEZE FILM BEARING DAMPERS

FLORIDA UNIVERSITY

PREPARED FOR
ARMY RESEARCH OFFICE-DURHAM

NOVEMBER 1974

DISTRIBUTED BY:
NTIS
National Technical Information Service
U. S. DEPARTMENT OF COMMERCE

DISCLAIMER NOTICE

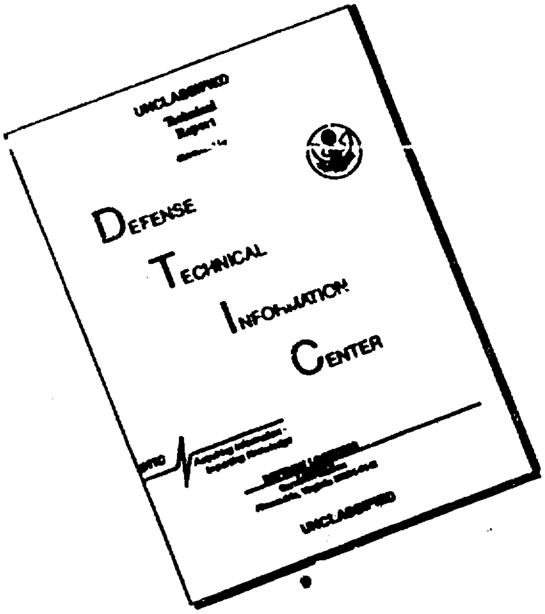

UNCLASSIFIED

Technical Report

DEFENSE TECHNICAL INFORMATION CENTER

UNCLASSIFIED

THIS DOCUMENT IS BEST QUALITY AVAILABLE. THE COPY FURNISHED TO DTIC CONTAINED A SIGNIFICANT NUMBER OF PAGES WHICH DO NOT REPRODUCE LEGIBLY.

REPORT DOCUMENTATION PAGE

READ INSTRUCTIONS BEFORE COMPLETING FORM

1. REPORT NUMBER	2. GOVT ACCESSION NO.	3. RECIPIENT'S CATALOG NUMBER AD/A-004020
4. TITLE (and Subtitle) PRELIMINARY INVESTIGATION OF THE DYNAMIC FORCE RESPONSE COEFFICIENTS FOR SQUEEZE FILM BEARING DAMPERS.		5. TYPE OF REPORT & PERIOD COVERED FINAL REPORT November 1, 73 - July 31, 74
		6. PERFORMING ORG. REPORT NUMBER
7. AUTHOR(s) John M. Vance and Alan J. Kirton		8. CONTRACT OR GRANT NUMBER(s) DAHC04-74-G-0048
9. PERFORMING ORGANIZATION NAME AND ADDRESS University of Florida Department of Mechanical Engineering Gainesville, FL 32601		10. PROGRAM ELEMENT, PROJECT, TASK AREA & WORK UNIT NUMBERS
11. CONTROLLING OFFICE NAME AND ADDRESS U. S. Army Research Office Box CM, Duke Station Durham, North Carolina 27706		12. REPORT DATE November 1974
		13. NUMBER OF PAGES 87
14. MONITORING AGENCY NAME & ADDRESS (if different from Controlling Office) USAAMROL Eustis Directorate Ft. Eustis, Va. 23604		15. SECURITY CLASS. (of this report) Unclassified
		15a. DECLASSIFICATION/DOWNGRADING SCHEDULE NA

16. DISTRIBUTION STATEMENT (of this Report)

Approved for public release; distribution unlimited.

17. DISTRIBUTION STATEMENT (of the abstract entered in Block 20, if different from Report)

NA

18. SUPPLEMENTARY NOTES

Reproduced by
NATIONAL TECHNICAL
INFORMATION SERVICE
U S Department of Commerce
Springfield VA 22151

19. KEY WORDS (Continue on reverse side if necessary and identify by block number)

Dampers, Bearings, Rotor Dynamics, Squeeze Film, Turbine Engines

20. ABSTRACT (Continue on reverse side if necessary and identify by block number)

An experimental study of the hydrodynamic force response of a squeeze film bearing damper with end seals was carried out. Measurements of the pressure distribution about a journal constrained to move in a circular orbit were made for the journal orbit centered in the annular clearance and offset from the center of the annular clearance. The effects of cyclic flow in a radial inlet were studied for the case of the journal orbit centered in the annular clearance.

PRICES SUBJECT TO CHANGE

For the off-center case, the pressure distribution around the damper was measured for four different combinations of eccentricity, radial velocity, and angular velocity of the line of centers, chosen in such a way as to allow calculation of the four bearing coefficients defined by Tondl. The experimentally determined pressure distributions were numerically integrated to determine the force components of the squeeze film. The results are compared to the "long bearing" and the "short bearing" solutions of Reynolds' equation. For the centered case, good agreement was found with the shape of the "long bearing" solution. Higher-than-predicted pressures and forces for light viscosity oil are explained by showing that this case is operating in the Taylor vortex flow regime. Similar calculations indicate that turbine engine dampers can also operate with vortex or turbulent flow.

TABLE OF CONTENTS

Page

LIST OF TABLES ii

LIST OF FIGURES iii

KEY TO SYMBOLS v

INTRODUCTION 1

THEORY OF THE HYDRODYNAMIC SQUEEZE FILM 12

EXPERIMENTAL EQUIPMENT AND METHODS 21
  Squeeze Film Apparatus 21
  Instrumentation 25
  Method of Data Analysis 26
  Experimental Procedure 30

RESULTS AND DISCUSSION 32
  Problems with the Squeeze Film Apparatus 32
  Centered Orbit Case 35
  Effect of Inlet Conditions 48
  Offset Orbit Case 52

CONCLUSIONS AND RECOMMENDATIONS 64
  Conclusions 64
  Recommendations 66

BIBLIOGRAPHY 68

APPENDIX I OIL VISCOSITY INFORMATION 69

APPENDIX II DIMENSIONS OF SQUEEZE FILM APPARATUS 71

APPENDIX III PRESSURE TRANSDUCER CALIBRATION INFORMATION 72

APPENDIX IV DESCRIPTION OF THE COMPUTER PROGRAMS USED IN DATA ANALYSIS 75

LIST OF TABLES

Table Page

1. Theoretical Force Components for "Long Bearing" and "Short Bearing" Solutions of Reynolds' Equation . . 18

2. Force Components for Centered Orbit Case 46

3. Force Components for Offset Orbit Case 62

LIST OF FIGURES

Figure Page

1. Squeeze Film Damper Operation 2

2. Typical Squeeze Film Damper Installation 3

3. Theoretical Model and Sign Convention 13

4. Squeeze Film Damper Apparatus Schematic 22

5. Squeeze Film Damper Apparatus Photograph 23

6. Squeeze Film Damper Apparatus and Instrumentation Photograph 27

7. Geometric Relationship Between $\overline{\Theta}$ and the Angular Position of the Eccentric Shaft 29

8. Circumferential Pressure Distribution, SAE 10 Oil, Transducer Position 0° 36

9. Circumferential Pressure Distribution, SAE 10 Oil, Transducer Position 90° 37

10. Circumferential Pressure Distribution, SAE 10 Oil, Transducer Position 180° 38

11. Circumferential Pressure Distribution, SAE 10 Oil, Transducer Position 270° 39

12. Circumferential Pressure Distribution, SAE 50 Oil, Transducer Position 0° 40

13. Circumferential Pressure Distribution, SAE 50 Oil, Transducer Position 90° 41

14. Circumferential Pressure Distribution, SAE 50 Oil, Transducer Position 180° 42

15. Circumferential Pressure Distribution, SAE 50 Oil, Transducer Position 270° 43

16. Circumferential Pressure Distribution, Unrestricted Inlet, Transducer Position 0° 59

17. Circumferential Pressure Distribution Unrestricted Inlet, Transducer Position 120° 50

18. Effect of Unrestricted Radial Inlet on "Long Bearing" Solution to Reynolds' Equation. 51

19. Angular Relationship Between the Pressure Transducer and Inlet. 53

20. Circumferential Pressure Distribution, Unrestricted Inlet, Transducer Position 0°. 54

21. Circumferential Pressure Distribution, Unrestricted Inlet, Transducer Position 180°. 55

22. Circumferential Pressure Distribution, Offset Eccentric Shaft Position 0°. 57

23. Circumferential Pressure Distribution, Offset Eccentric Shaft Position 90°. 58

24. Circumferential Pressure Distribution, Offset Eccentric Shaft Position 180°. 59

25. Circumferential Pressure Distribution, Offset Eccentric Shaft Position 270°. 60

26. Transducer Calibration Curve, 0-100 psig. 73

27. Transducer Calibration Curve, 0-200 psig. 74

KEY TO SYMBOLS

Letter Symbols

c	radial clearance
D_b	diameter of bearing
D_j	diameter of journal
e	journal eccentricity
F_x	tangential force component
F_y	radial force component
$F_1(n)$	force coefficient of radial force component due to ω_c
$F_2(n)$	force coefficient of radial force component due to $\dot{n}$
$F_3(n)$	force coefficient of tangential force component due to ω_c
$F_4(n)$	force coefficient of tangential force component due to $\dot{n}$
h	oil film thickness
L	length of journal
n	journal eccentricity ratio (e/c)
$\dot{n}$	dn/dt
p	pressure
p_o	pressure at maximum film thickness
r_j	radius of journal
t	time
U_o	velocity of x_1, x_3 plane
U_1	velocity in x_1 direction

V	surface velocity used in transition parameter
X_1	distance measured on one surface in direction of relative motion
X_2	distance measured at right angles to the surface
X_3	distance measured on the surface at right angles to relative motion

Greek Symbols

Θ	angle measured from maximum film thickness
$\overline{\Theta}$	angle measured from maximum film thickness to the pressure transducer
$\overline{\Theta_I}$	angle measured from maximum film thickness to the inlet
μ	oil viscosity
ψ	angle of eccentric shaft from vertical up position
ψ_o	angle of pressure transducer from vertical up position
ω_b	angular velocity of bearing
ω_c	angular velocity of line of centers
ω_j	angular velocity of journal

Dimensionless Groups

$\dfrac{p - p_o}{\mu r_j^2 \omega_c / c^2}$	dimensionless pressure
$\dfrac{Vc\rho}{\mu} \sqrt{\dfrac{c}{r_j}}$	transition parameter (Ref. 8)

INTRODUCTION

A major problem facing designers and manufacturers of high speed turbine engines is the vibration and dynamic loads caused by rotor shaft unbalance. The wider range of rotational speeds and the use of longer shafts in multi-spool engines has made this problem more acute. Moreover, the use of more flexible bearing supports in controlling the location of the critical speeds allows the dynamic forces to have a greater effect upon rotor shaft excursions.

In order to alleviate this problem manufacturers of several new turbine engines have incorporated squeeze film dampers in the rotor shaft bearing supports. The experience of these manufacturers indicates that the use of squeeze film dampers significantly reduces engine vibrations and lowers engine rejection rates due to rotor shaft unbalance. Experimental studies by Cooper [1] and White [2] of rotor shafts supported by squeeze film dampers have shown the effect of the squeeze film in decreasing vibratory loads and in increasing the region of shaft stability. It has also been shown [3,4] that external damping can suppress non-synchronous whirl at super critical speeds. A review of this and other research will be made later in this section.

The squeeze film damper configuration is relatively simple. A schematic diagram showing the operation of a squeeze film is shown in Figure 1. A typical installation of a squeeze film damper is shown in Figure 2. The outer race of the rolling element bearing is fitted loosely in the bearing support structure. The radial clearance may range from .01 to .0005 of the bearing radius, depending upon the design. Radial motion of the bearing outer race is permitted but rotation is prevented using some type of mechanical constraint. The annular clearance,

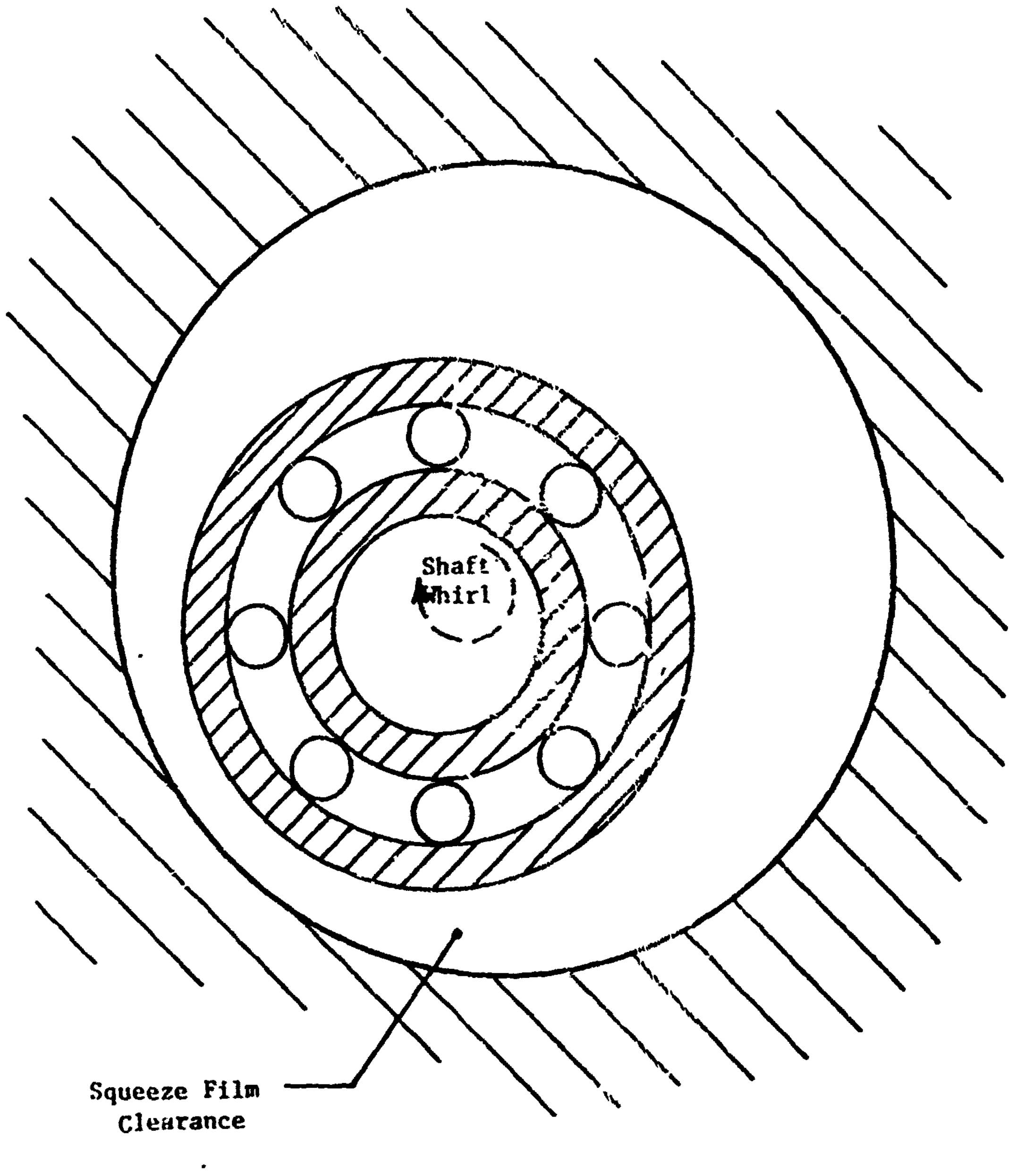
Shaft
Whirl
Squeeze Film
Clearance

FIGURE 1. Squeeze Film Damper Operation

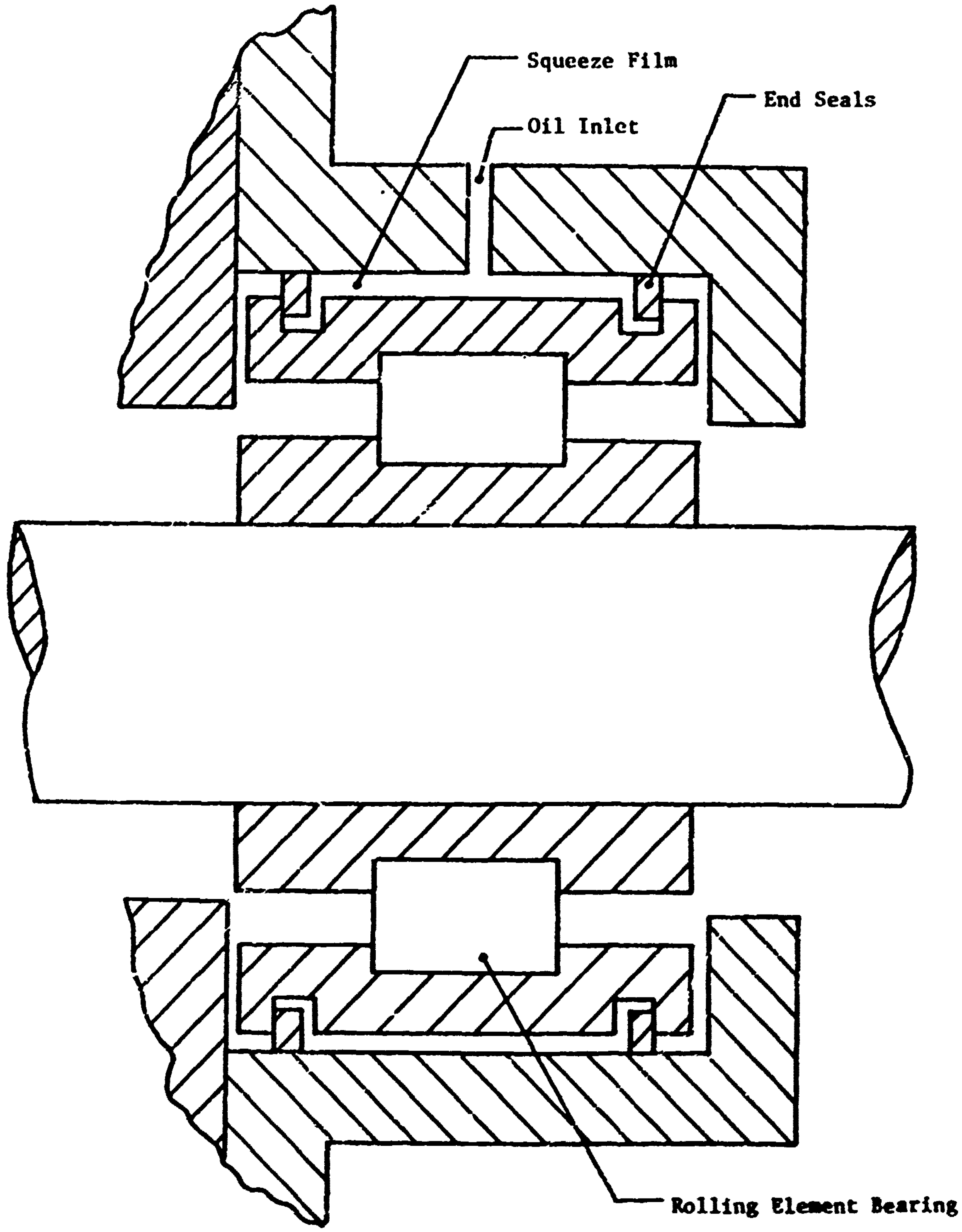
Squeeze Film
End Seals
Oil Inlet
Rolling Element Bearing

FIGURE 2. Typical Squeeze Film Damper Installation

between the bearing outer race and the housing, is filled with oil. The dynamic forces acting on the bearing will result in an orbital motion of the bearing outer race. This motion produces corresponding hydrodynamic forces in the squeeze film which oppose the shaft motion and rotor dynamic forces. Thus the squeeze film acts as a complex spring and damper system which, if properly designed, will significantly reduce the forces transmitted to the bearing supports. However, it has also been shown [2, 5] that an improperly designed squeeze film damper can magnify the forces transmitted to bearing supports. Thus the result is a worse situation than if the bearings were mounted in rigid supports.

In order to correctly design a squeeze film damper it is necessary to predict the hydrodynamic forces in the squeeze film as a function of the shaft motion and pertinent squeeze film parameters. The rotor dynamics of the shaft supported by squeeze film dampers may then be predicted and the squeeze film parameters modified to obtain the desired damping of the rotor motion and forces. These parameters include the length-diameter ratio, the eccentricity-clearance ratio, fluid viscosity, and supply pressure. The effect of the inlet conditions, cavitation and end seals must also be determined.

In order to predict the force coefficients of the squeeze film the pressure distribution throughout the film must be determined. Analytical and experimental studies of journal bearings have resulted in several different theories for predicting the pressure distribution in journal bearings. The theoretical model of squeeze film dampers and journal bearings are identical, except that no existing journal bearing theory takes into account the boundary conditions produced by end seals. Since end seals reduce or eliminate axial flow, it may be surmised that the "long bearing" theory would fit this case more closely than the "short bearing" theory.

The theoretical work developed for journal bearings may be applied to squeeze film dampers if it can be determined that the boundary conditions are similar or produce similar results.

It was the purpose of this study to make an experimental investigation of the hydrodynamic squeeze film. The object, in designing the experimental rig, was to duplicate, as closely as possible, the configuration found in turbine engines, while keeping the measurements as simple as possible.

The use of end seals in the test rig allowed investigation of their effect upon the pressure distribution. Many squeeze film damper designs and some journal bearing installations contain end seals to minimize end leakage, yet little analytical or experimental work has been accomplished to determine their effect on the hydrodynamic film pressures.

Initial measurements and observations showed that it was also desirable to study the effect of the inlet conditions. The inlet design of the experimental rig and some squeeze film dampers do not meet the boundary conditions imposed by any existing theory. Thus the effect of varying inlet conditions was included in this investigation.

The oil supply pressure was adjusted so as to maintain a positive pressure throughout the film. Cavitation was thereby prevented and a full 360 degree film was developed. Although cavitation does occur in practice for both journal bearings and squeeze film dampers, the uncavitated case provides the basis for understanding the effects of cavitation. Later research will cover the case of the cavitated film.

The experimental rig also has the capacity to study the pressure distribution for the case of the eccentricity being a nonconstant function of time. Little or no research has been carried out for this case, although this is the condition found in any journal bearing or squeeze film damper with a varying load. The rotor shaft of any turboshaft or turbojet engine operated in a horizontal position will whirl about an equilibrium point below the centerline of the bearing dampers, due to the effect of gravity. Inertia forces due to vehicle maneuvers can deflect the orbit center even further. Centering springs are often used to prevent contact with the damper bearing wall, but these are made as soft as practical to keep the rigid-body critical speeds low. The off center orbit, even if circular, produces both non-zero radial velocities and non-constant angular velocities of the line of centers. If the orbit can be assumed small, it is common practice to transform the response forces from the rotating coordinates into inertial (fixed) coordinates and calculate "linearized" stiffness and damping coefficients for a rotor dynamics analysis of the motion "in the small".

The actual size of the whirl orbit depends on the magnitude of rotor unbalance, or on the magnitude of any destabilizing self-excited forces induced by the motion. Since the damper force response is nonlinear, the orbit size is a critical factor in the analysis. The type of analysis to be performed (e.g. linearized, steady-state, nonlinear, transient) should be determined by the primary purpose of the damper, which is usually one of the following:

(a) To reduce synchronous response to rotor unbalance for the expected range of unbalance in production engines, thus reducing rejections due to excessive vibration.

(b) To increase reliability and flight safety by reducing the response to sudden and abusive unbalance, such as caused by the loss of a turbine blade.

(c) To suppress nonsynchronous whirl and self-excited dynamic instabilities, such as caused by internal friction in the rotor-shaft assembly.

Most damper and rotor dynamics analysis performed to guide engine design has been aimed at objective (a). This objective can usually be met satisfactorily by a design based on a small orbit (linearized) analysis, as described above, or on a centered circular orbit analysis in which the damping and stiffness coefficients are constant in the rotating coordinates.

It is becoming increasingly clear that more effort must be directed toward objectives (b) and (c). By definition, a rotor dynamics analysis to meet objective (b) must consider large, off center, whirl orbits with non-zero radial velocities. To be complete, a stability analysis to meet objective (c) should consider both small and large motions. A transient marching solution of the complete equations by digital computer is the only method capable of yielding accurate results for some of these cases, but the results can be no more accurate than the force response prediction model for the dampers.

In light of the above, a basic objective of the work reported here was to develop an experimental capability to measure damper pressures and forces for both the case of a constant and time varying eccentricity (non-zero radial velocity), so as to determine the validity of existing theories for use as a prediction model.

As will be described in a later section, the resulting experimental rig produces circular orbits, with a variable amount of offset from the damper center. It is felt that little generality is lost by the circular constraint. Although there are an infinity of orbit shapes which can be and are produced by engine rotors, any point on any shape orbit can be uniquely described by the instantaneous eccentricity, radial velocity, and angular velocity of the line of centers. These latter quantities are all reproducible by the circular orbit rig with the proper amount of offset.

It is appropriate at this time to briefly survey some of the analytical and experimental research that has been accomplished by other investigators related to this study.

Cooper [1] was one of the first investigators to study the effect of the bearing supports upon the rotor dynamics. In an experimental study he demonstrated the use of oil films in controlling shaft vibrations.

In Cooper's initial tests a stiff shaft was supported by gas bearings. The effect of limiting the orbit amplitude using mechanical stops was studied first. The orbit amplitude was then limited using a hydrodynamic oil film.

It was found that limiting the journal orbit using mechanical stops caused violent pounding of the stops and instability of the shaft motion. Introduction of the hydrodynamic oil film caused smooth running of the shaft until the onset of oil-whirl as the shaft rotational speed reached twice the shaft critical speed.

The shaft was then supported using rolling element bearings mounted in squeeze film dampers. These tests resulted in smooth running of the rotor without the problem of oil-whirl. These tests also showed the existence of two stable orbits, the larger being characterized as a whirl mode and the smaller characterized as being the inverted mode.

White [2], extending the work of Cooper, studied the dynamics of a simple rigid shaft mounted in squeeze film dampers. A theoretical analysis, representing the squeeze film by the "short bearing" solution of Reynolds' equation, considered the stability of the three predicted bearing center orbits.

It was shown that the intermediate eccentricity orbit is always unstable and that the whirl (large) and inverted (small) orbits are always stable. The whirl condition was found to be undesirable as it increased the forces transmitted to the bearing supports.

An apparatus designed to simulate the theoretical model was constructed. The existence of the two stable equilibrium orbits was observed. It was noted that there were speed ranges over which either orbit could exist for a particular out-of-balance. It was clearly shown that for the whirl orbit, the rotor mass center was more distant from the center of rotation, thus the squeeze film effectively increased the unbalance.

In similar research Mohan and Hahn [5] also predicted the two stable orbits using the "short bearing" analysis to describe the squeeze film. The inverted mode was characterized by a low transmissibility, less than one, while the whirl mode commonly had a transmissibility greater than one. A critical shaft unbalance was found, above which only the whirl mode was stable and the transmissibility was greater than one. Design graphs were presented to aid in the design of squeeze film dampers over a wide range of operating conditions.

Vance and Lee [3] performed a stability analysis of high speed rotors with internal friction. It was shown that the threshold speed of instability for nonsynchronous whirl induced by the internal friction depends on the ratio of internal friction to external damping. It was also shown that when the external damping exceeds the internal friction, operating speeds up to eighty percent greater than the critical speed may be safely attained. Conversely, when the internal friction is many times larger than the external damping the stability speed threshold approaches the critical speed. It may be inferred that correctly designed squeeze film bearing dampers can provide the external damping required for safe operation above the critical speed.

Sweet and Genin [4], in an analytical study, demonstrated that the journal bearing instability known as "oil whip" may be eliminated by a sufficient amount of external damping. However, the magnitude of external damping required to significantly alter the undamped results is much too large to be produced by normal external dissipative forces. It was then shown that a squeeze film damper around the bearing can supply the necessary external damping to eliminate the instability due to oil whip.

The above studies were, for the most part, concerned about the effect of the hydrodynamic film upon the dynamics of the rigid rotor. The nature of the hydrodynamic film was not studied. The theories that were used to predict the film forces have not yet been experimentally verified.

Thomsen and Anderson [6], in an experimental study, investigated the hydrodynamic squeeze film. A vertical shaft was used, with the upper rolling-element bearing mounted in a centrally preloaded squeeze film damper. The excitation force was provided by deliberately creating an unbalance in the shaft. The squeeze film damping coefficient was obtained by measuring the deflection in the radial supports of the bearing housing. The investigation was primarily intended to study the range of damping available from the squeeze film by varying radial clearance and oil viscosity.

Potential errors are incurred in determining the squeeze film forces by measuring the deflection of the housing supports, due to the effect of the inertia of the housing, which can be significant. Also, deflection of the housing alters the squeeze film geometry, introducing another potential source of error.

Jones [7] investigated the fundamental hydrodynamics of the squeeze film. The axial and circumferential pressure distribution of the squeeze film were measured about a journal constrained to move in a circular orbit around the housing center. The design of the rig was such as to approximate the boundary conditions of the "short bearing" theory. Oil was provided to the squeeze film through a central circumferential groove. Cavitation was allowed in the divergent part of the squeeze film. The parameters varied during the tests were the film geometry, journal eccentricity ratio, orbital speed and the supply pressure.

It was found that the cavitated, "short bearing" theory provided a reasonably good approximation to the results from the experiments. Jones' study gives good insight into the squeeze film hydrodynamics for damper configurations which approximate the boundary conditions of the "short bearing" theory.

There has been little research of the rotor dynamics or squeeze film hydrodynamics for configurations approximating the "long bearing" theory. This is especially true for the case of a non-constant eccentricity (i.e. non-zero radial velocity).

All of the research discussed above is based on Reynolds' theory for laminar flow. Squeeze film dampers may operate in different flow regimes. Vohr [8] investigated the fluid flow between nonconcentric rotating cylinders (no orbiting). The object of the investigation was to study the nature of Taylor vortex flow and turbulence in concentric and eccentric annuli. Criteria were developed as a function of the Reynolds' number and Taylor number for the onset of Taylor vortices. Although the results may not be quantitatively applicable to squeeze film flow, they do suggest that the possibility of flow transition is a critical question to be considered.

THEORY OF THE HYDRODYNAMIC SQUEEZE FILM

The equations governing the hydrodynamics of the squeeze film were developed largely from the theory describing journal bearings. The theoretical model and sign convention are shown in Figure 3.

The general equation for the hydrodynamic film between two flat surfaces was developed by Reynolds.

$$\frac{\partial}{\partial x_1}\left(h^3\frac{\partial p}{\partial x_1}\right) + \frac{\partial}{\partial x_3}\left(h^3\frac{\partial p}{\partial x_3}\right) = 6\mu\left\{\frac{\partial}{\partial x_1}\left[(U_0 + U_1)h\right] + 2\frac{\partial h}{\partial t}\right\}$$

Implicit in the above equation are Reynolds' assumptions of laminar flow, incompressibility, constant viscosity, and that the inertia and body forces are negligible. It is also assumed that at the lubricated surfaces the fluid has the velocity of the surfaces and that at the film extremities the pressure depends upon the external conditions.

It should be noted that end seals do not meet the boundary conditions imposed by Reynolds' equation. The end seals prevent the pressure at the film extremities from approaching the external conditions. The end seals also constrain the velocities at the extremities to equal the velocity of the seals.

Reynolds' equation may be written in terms of the squeeze film parameters, defined in Figure 3 and the List of Symbols.

$$\frac{\partial}{\partial\theta}\left[(1 + n\cos\theta)^3\frac{\partial p}{\partial\theta}\right] + r_j^2\frac{\partial}{\partial x_3}\left[(1 + n\cos\theta)^3\frac{\partial p}{\partial x_3}\right]$$

$$= \frac{12\mu r_j^2}{c^2}\left[\omega_c\sin\theta + \dot{n}\cos\theta\right]$$

In the derivation of this equation it is assumed that the effect of the curvature is negligible and certain assumptions are made concerning the

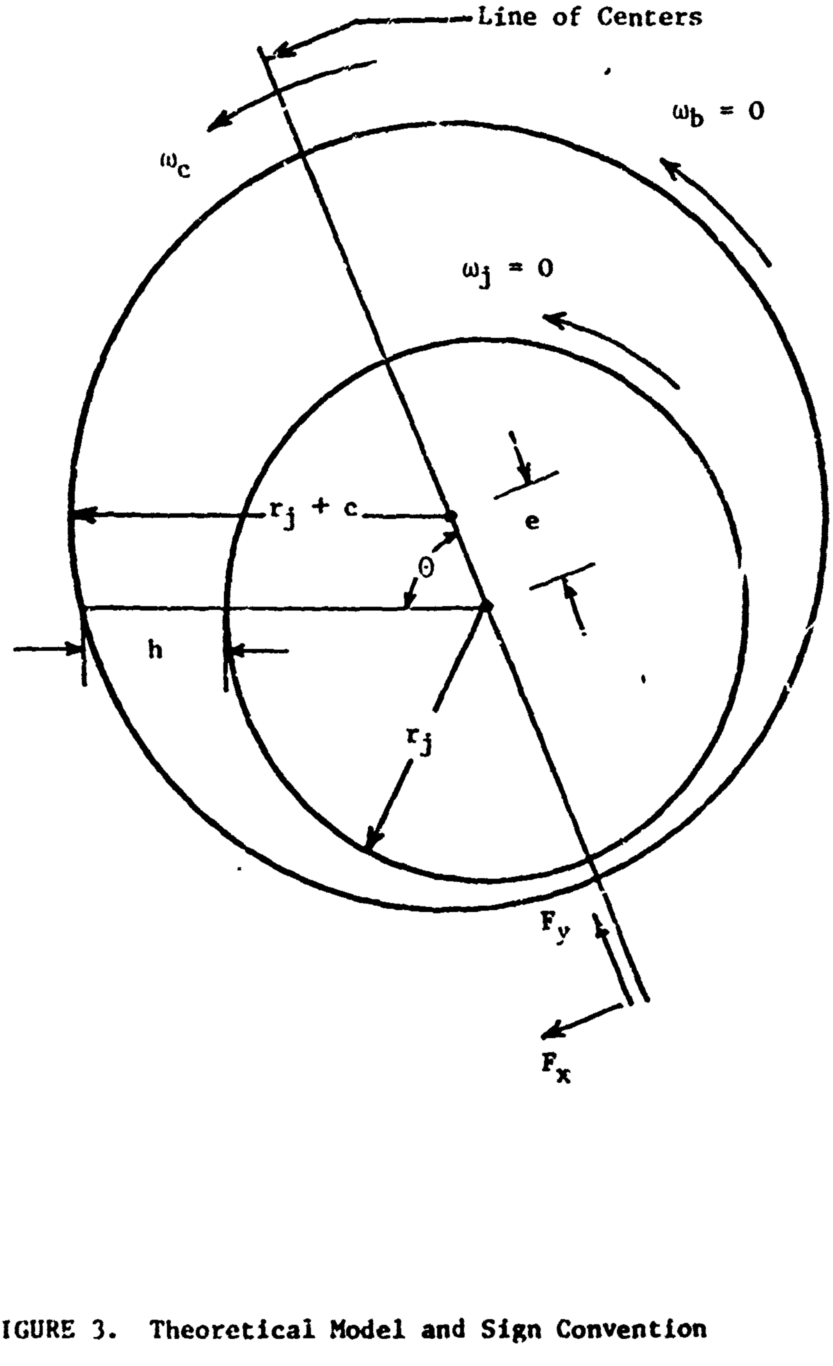

Line of Centers
$\omega_b = 0$
ω_c
$\omega_j = 0$
$r_j + c$
e
Θ
h
r_j
F_y
F_x

FIGURE 3. Theoretical Model and Sign Convention

relative size of some of the geometric ratios.

An analytical solution to Reynolds' equation has never been obtained. Although numerical solutions have been obtained, they are considered here to be too unwieldy for use in predicting the damper forces in a useful form for rotor dynamics analysis. The equations can be considerably simplified by either of two approximations, both of which involve the length of the bearing and the amount of fluid flow in the axial direction.

If the fluid film is assumed to be infinitely long in the x_3 direction the variation of the film properties in that direction will be negligible. Thus the second term on the left hand side of Reynolds' equation may be neglected. This is the "long bearing" assumption and is the basis of Sommerfeld's solution for journal bearings.

The simplified Reynolds' equation obtained by this assumption must then be integrated twice with respect to θ to obtain the pressure distribution. This integration requires the choice of two boundary conditions. In the theory developed by Sommerfeld one of these conditions specifies that the pressure at $\theta=0$ be a reference pressure, p_0. For the case of a radial inlet located centrally in the oil film the validity of this assumption should be questioned. In a journal bearing under a constant load the inlet position would not vary with respect to θ and the assumption would seem to be valid. In a squeeze film damper, however, the line of centers (the line passing through the center of the journal and the center of the housing) is constantly rotating. Thus the position of the inlet is constantly changing with respect to θ. The effect of this upon the pressure distribution is dependent upon the ability of the inlet flow to dynamically follow the changing pressures throughout each cycle. A more elaborate discussion of this problem is contained in the section containing the experimental results.

The result of the second integration is an expression for the circumferential pressure distribution about the journal. Trumpler [9], using this method of analysis, obtains the following expression for the pressure distribution:

$$p-p_0 = \frac{6\mu r_j}{c^2}\{-2\omega_c(\frac{n}{2+n^2})\ \frac{\sin\theta(2+n\ \cos\theta)}{(1+n\ \cos\theta)^2} + [\frac{1}{(1+n\ \cos\theta)^2} - \frac{1}{(1+n)^2}]\ \frac{\dot{n}}{n}\}$$

The alternative simplifying assumption concerning Reynolds' equation is that the fluid film is infinitely short in the x_3 direction. Thus the variation of the film properties in that direction predominate and the first term on the left hand side of Reynold's equation may be neglected. This is the basis of Dubois' and Ocvirk's [10] solution for journal bearings and is known as the "short bearing" assumption.

The simplified equation obtained using this assumption is then integrated twice with respect to x_3 to obtain the pressure distribution. Again, this integration requires two boundary conditions. These specify that the pressure at each end of the film is equal to the supply pressure. In practice the oil is usually supplied to the film through a central, circumferential groove and the ends of the film are at atmospheric pressure. Unless the lubricant is supplied at near atmospheric pressure, the use of a central supply groove does not meet the specified boundary conditions. It is evident that the use of end seals would violate these boundary conditions to an even greater extent.

The result of this integration is an expression for the pressure distribution in the circumferential and axial directions. Jones [7], using this analysis, obtains (modified for the sign convention used in this study):

$$p - p_0 = \frac{6\mu}{c^2} \frac{(\dot{n} \cos\theta + \omega_e n \sin\theta)}{(1 + n \cos\theta)^3} (x_3^2 - \frac{L^2}{4})$$

Neither the "long bearing" theory nor the "short bearing" theory is entirely accurate for bearings of finite length. The "short bearing" assumption is usually considered valid for length/radius ratios less than two while the "long bearing" theory is considered valid for length/radius ratios greater than two. Regardless of length, a journal bearing or squeeze film damper equipped with end seals may approximate the "long bearing" theory in that flow in the axial direction is prevented.

The pressure distribution obtained using either the "short bearing" assumption or the "long bearing" assumption may be integrated to obtain the radial and tangential force components of the squeeze film.

Using the "long bearing" theory the pressure distribution is integrated with respect to θ.

$$F_x = -Lr_j \int_{\theta_1}^{\theta_2} p \sin\theta \, d\theta$$

$$F_y = -Lr_j \int_{\theta_1}^{\theta_2} p \cos\theta \, d\theta$$

For the "short bearing" theory the pressure distribution is integrated with respect to θ and x_3.

$$F_x = -Lr_j \int_{\theta_1}^{\theta_2} \int_{-L/2}^{L/2} p \sin\theta \, dx_3 d\theta$$

$$F_y = -Lr_j \int_{\theta_1}^{\theta_2} \int_{-L/2}^{L/2} p \cos\theta \, dx_3 d\theta$$

These integrations require a further assumption regarding the circumferential length of the squeeze film. Both solutions to Reynolds' equation predict significant negative pressures, with respect to the supply pressure, in the divergent half of the squeeze film ($0 \leq \theta \leq \pi$). However, the lubricant film cannot support negative pressures, as vaporization of the lubricant will occur. Thus the solutions of Reynolds' equation are valid only if the supply pressure is sufficiently high to prevent cavitation. For this case the pressure distribution is integrated from $\theta=0$ to $\theta=2\pi$ to give the force components for the full film.

If the supply pressure is not sufficiently high to support a full film then the film will be cavitated over part of the circumference. The pressure in this region cannot fall below the vapor pressure of the lubricant and may be assumed to equal either the vapor pressure or atmospheric pressure. For this case the most common assumption is that the pressure in the divergent part of the film is equal to atmospheric pressure while the pressure in the convergent part of the film ($\pi < \theta < 2\pi$) is given by the solution to Reynolds' equation. Integration using these limits results in the force components for the cavitated film.

Expressions for the force components, using this method of analysis, for the "long bearing" and the "short bearing" solutions to Reynolds' equation, with full and cavitated films, are given in Table 1.

Other researchers have obtained different expressions for the force components.

Tondl[11] divides the squeeze film force into four force coefficients. The force components are presented in the form:

$$F_x = -6\mu L \frac{r_j^3}{c^2} \left[(-2\omega_c) F_3(n) + 2\dot{n} F_4(n) \right]$$

$$F_y = 6\mu L \frac{r_j^3}{c^2} \left[(-2\omega_c) F_1(n) + 2\dot{n} F_2(n) \right]$$

Film Extent	Force Component	Film Length Assumption	
		"Long Bearing"	"Short Bearing"
Full (0 to 2π)	F(x)	$24\pi\mu L \frac{r_j^3}{c^2} \frac{\omega_c n}{(2+n^2)\sqrt{1-n^2}}$	$\pi\mu r_j \frac{L^3}{c^2} \frac{n}{(1-n^2)^{3/2}}$
	F(y)	$12\pi\mu L \frac{r_j^3}{c^2} \frac{\dot{n}}{(1-n^2)^{3/2}}$	$\pi\mu r_j \frac{L^3}{c^2} \frac{(1+2n^2)\,\dot{n}}{(1-n^2)^{5/2}}$
Cavitated (π to 2π)	F(x)	$12\mu L \frac{r_j^3}{c^2} \frac{2\dot{n}}{(1+n)(1-n^2)} + \frac{\omega_c \pi n}{(2+n^2)(1-n^2)^{1/2}}$ $+2r_j L p_o$	$\mu r_j \frac{L^3}{c^2} \frac{2n\dot{n}}{(1-n^2)^2} + \frac{\pi}{2} \frac{\omega_c n}{(1-n^2)^{3/2}} + 2r_j L p_o$
	F(y)	$6\mu L \frac{r_j^3}{c^2} \frac{\dot{n}\pi}{(1-n^2)^{3/2}} + \frac{4\omega_c n^2}{(2+n^2)(1-n^2)}$	$\mu r_j \frac{L^3}{c^2} \frac{\pi}{2} \frac{\dot{n}(1+2n^2)}{(1-n^2)^{5/2}} + \frac{2\omega_c n^2}{(1-n^2)^2}$

TABLE 1. Theoretical Force Components for the "Long Bearing" and "Short Bearing" Solutions to Reynolds Equation

The preceding form is useful as it separates the contributions of the radial and orbital motion of the journal, to the radial and tangential force components. In his analysis, Tondl calculates the force components directly without first determining the pressure distribution. However, in determining the location of the point of maximum pressure, Tondl implicitly makes the assumption of zero $\dot{n}$. This would invalidate the results for the case of a non-zero $\dot{n}$.

Hori [12], in an analysis describing journal motion during oil whip, also formulates force components which would be applicable to a squeeze film damper. However, certain assumptions are made concerning surface velocities which are true only for $\dot{n} = 0$.

Lund and Saibel [13] divide the force components into eight coefficients in cartesian coordinates. The coefficients are in the form of spring and damping constants:

$$K_{xx} = \frac{-\partial F_x}{\partial x} \qquad K_{xy} = \frac{-\partial F_x}{\partial y} \qquad K_{yy} = \frac{-\partial F_y}{\partial y} \qquad K_{yx} = \frac{-\partial F_y}{\partial x}$$

$$B_{xx} = \frac{-\partial F_x}{\partial \dot{x}} \qquad B_{xy} = \frac{-\partial F_x}{\partial \dot{y}} \qquad B_{yy} = \frac{-\partial F_y}{\partial \dot{y}} \qquad B_{yx} = \frac{-\partial F_y}{\partial \dot{x}}$$

Coefficients in the above form allow the designer to simulate the dynamics of the rotor-bearing-damper support system and use a numerical marching solution to study the transient response.

However, such solutions are of little use without confidence in the theories used to obtain the force coefficients. Current literature is not consistent in the development of equations applicable to squeeze film dampers, especially in the case of a non-zero $\dot{n}$. The basic assumptions upon which Reynolds' equation is based should be questioned for many squeeze film damper installations. Vohr [8] developed criteria for vortex and turbulent flow between nonconcentric rotating cylinders. Applying these criteria to one squeeze film damper installation indicates that the flow is turbulent, thus making an analysis based on Reynolds' equation invalid.

The high rotational speeds and the low viscosity oil used in many squeeze film damper installations make Reynolds' assumption of laminar flow questionable. A further discussion of this topic is carried out in a later section.

EXPERIMENTAL EQUIPMENT AND METHODS

In designing the experimental rig it was desired to duplicate the configuration of squeeze film damper designs found in many turbine engines, while taking advantage of the theory of similitude to allow the use of a larger clearance (to minimize the effect of manufacturing tolerances) and to allow operation at lower speeds.

The objective of the design was to provide a journal with a known, constrained motion within an annular clearance filled with oil. In this way the squeeze film could be studied independently from the dynamics of the rotor-bearing-support system.

It was decided to measure the pressure distribution in the oil film instead of measuring the resultant film forces. The pressure measurements allow a more direct check of the existing squeeze film theories and the film forces are easily calculated from the pressure distribution. The film forces would have to be determined by measuring the housing deflection and it would be difficult to determine the effect of the housing inertia on these measurements.

Squeeze Film Apparatus

A schematic diagram of the basic rig is shown in Figure 4. A photograph of the actual hardware is shown in Figure 5.

The journal is mounted on the eccentric lobe of a stiff shaft using ball bearings. The shaft rotates on ball bearings mounted in rigid supports.

The outer housing is supported by end plates using locational fits in order to allow it to rotate through 360 degrees. The housing is indexed in 10-degree increments and a pin is inserted in order to keep it from rotating. Holes are tapped in the outer cylinder for installation

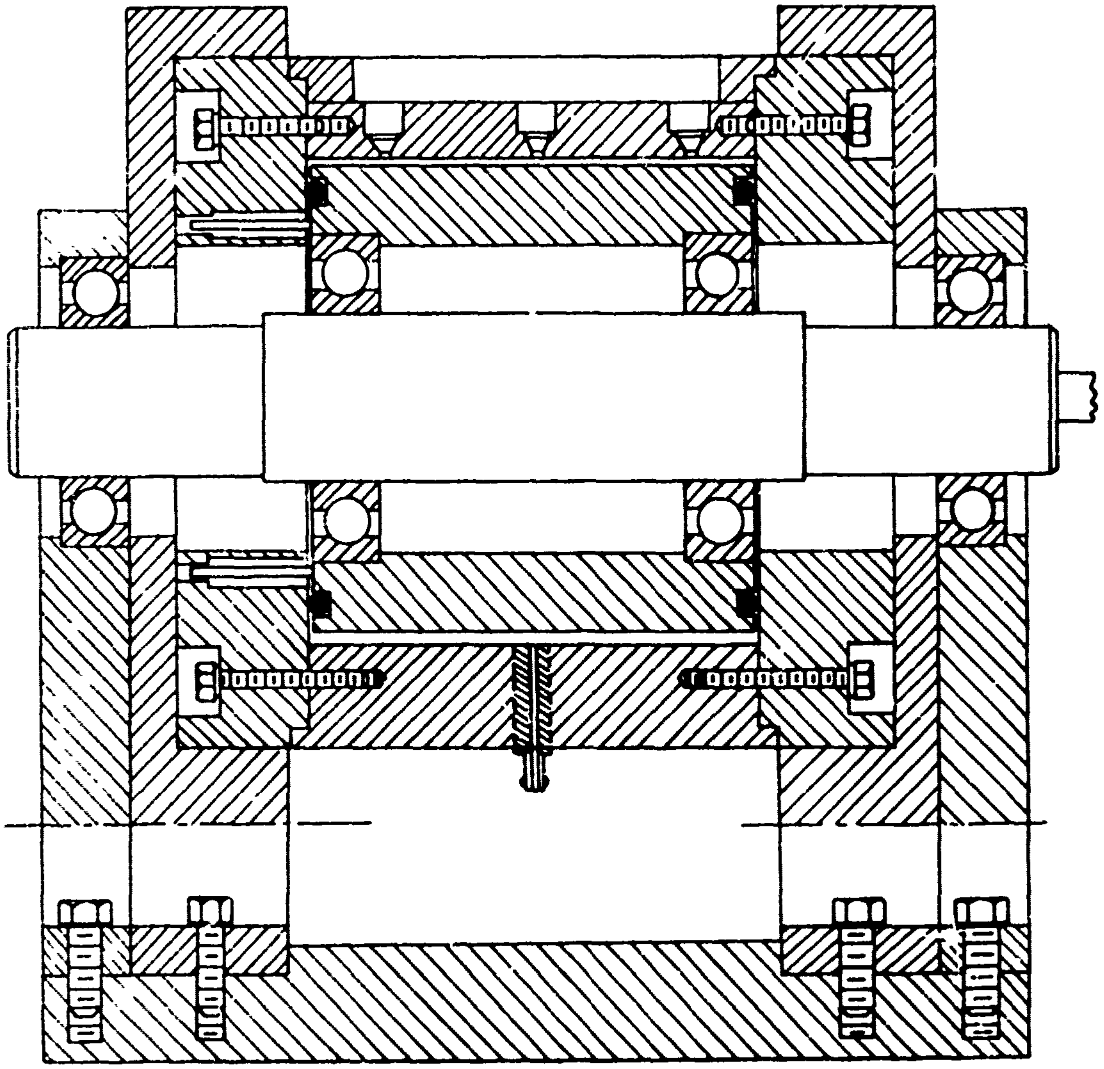

FIGURE 4. Squeeze Film Damper Apparatus Schematic

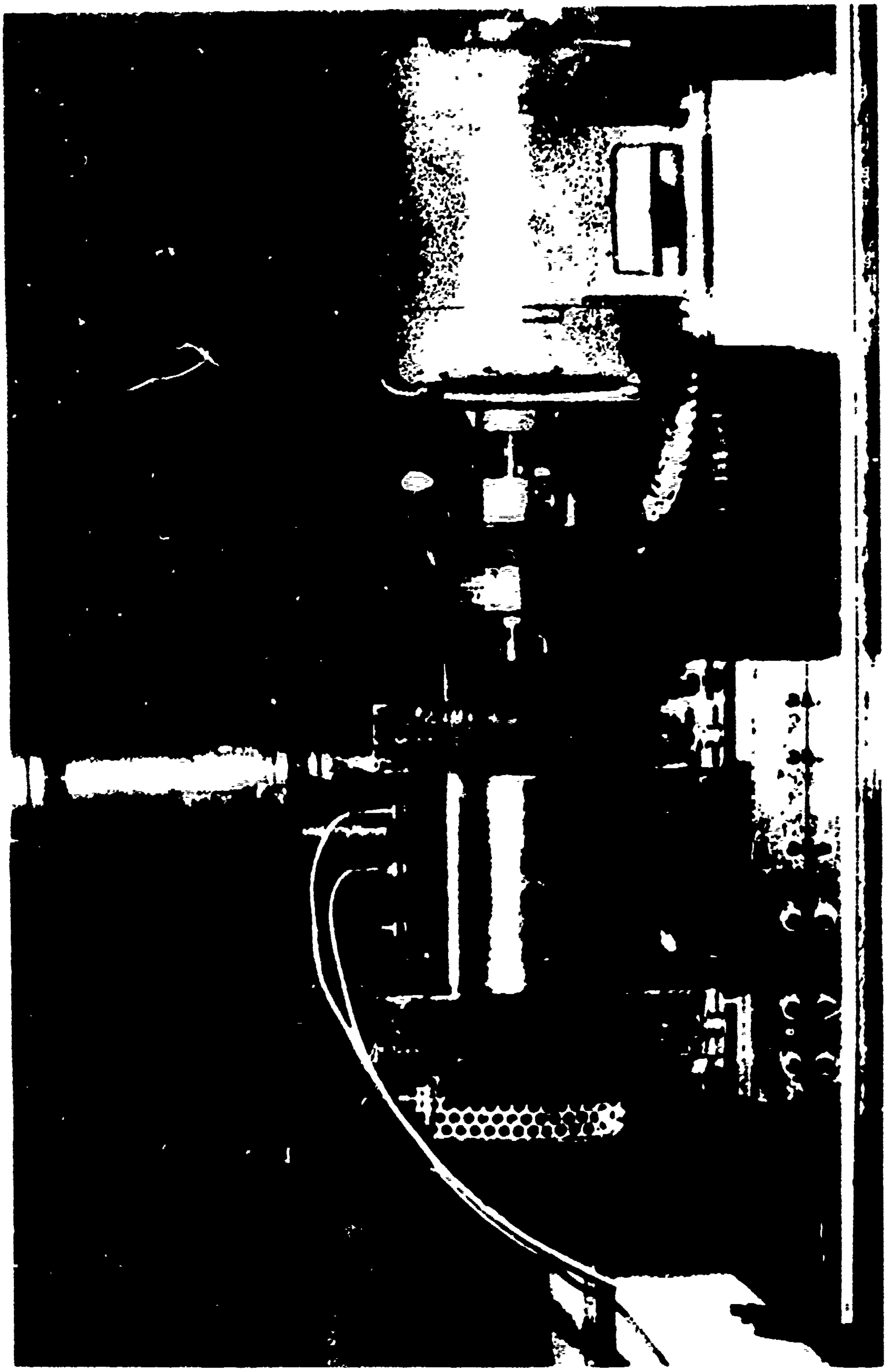

FIGURE 5. Photograph of Experimental Rig

Reproduced from best available copy.

of pressure transducers and a thermocouple. These are in direct contact with the oil film. Rotation of the outer housing allows the circumferential pressure distribution to be determined using one pressure transducer.

The journal is pinned to the outer housing using four axial pins. These pins allow radial and orbital motion of the journal but prevent relative rotation between the journal and housing.

Oil is supplied to the squeeze film through an orifice located centrally in the outer housing, 140° from the pressure transducers and thermocouple. The orifice size was varied on several tests to determine the effect of differing inlet conditions upon the pressure distribution. The oil is supplied under pressure using compressed air and a pressure regulator.

Two oils of differing viscosity were used during the experimentation. Viscosity information on the oils is given in Appendix I.

The ends of the journal are sealed against the end plates using 'o' rings to prevent axial flow of the oil. Leakage past the 'o' rings was minimal.

The eccentric shaft is driven by an electric motor using a flexible coupling to prevent axial loads on the journal. The rotational speed of the motor was fixed at 1765 revolutions per minute.

The eccentric shaft, hence center of the journal orbit, can be offset from the center of the outer housing by installing shims under the eccentric shaft supports. In this way the eccentricity of the journal orbit, relative to the center of the housing, varies throughout each cycle and a known $\dot{n}$ is obtained. Separate tests were carried out with the eccentric shaft centered and offset from the housing center.

Static balance of the eccentric shaft and journal was accomplished by the addition of a counterweight at one end of the shaft.

The basic dimensions of the test rig pertinent to squeeze film calculations are given in Appendix II.

Instrumentation

Four holes are tapped in the outer housing for installation of pressure transducers. During the tests Viatran Model 210 strain gage type pressure transducers were used with ranges of 0 to 100 psig and 0 to 200 psia. The natural frequency of the transducers is 20 kilocycles/second and the response time is 500 microseconds to reach 90% of full scale output. The pressure transducer was calibrated using a dead weight tester manufactured by Amthor Testing Instrument Company. The resulting calibration curves are given in Appendix III. The transducer is connected to the oil film through a short cylindrical tapping in the outer housing. The resulting dead volume was assumed to have a negligible effect on the dynamic pressure readings. To obtain the circumferential pressure distribution the outer housing was rotated through 360 degrees in 10 degree increments.

The pressure transducer was powered using a ten volt battery power supply. The output from the transducer was displayed on a Type 561 B Tektronix Oscilloscope after being amplified by a Type 3A3 Dual-Trace Differential Amplifier. The signal was displayed versus a time sweep generated by a Type 2B67 Time Base.

The time sweep was triggered externally using the amplified signal from a Type MM0002 Bruel and Kjaer magnetic transducer. The signal was amplified using a Bell and Howell Model 1-165 DC amplifier. The time sweep was triggered each time the lobe of the eccentric shaft was in the vertical up position. The positioning of the transducer was determined by using the amplified signal to trigger a strobe light. The instantaneous position of the shaft at the time of triggering could then be determined and the tranducer moved to bring the lobe to the vertical up position.

A knowledge of the oil temperature of the squeeze film was desired in order to make an accurate determination of the oil viscosity. This was accomplished by mounting a copper-constantan thermocouple in a pressure fitting and installing it in one of the holes provided for the pressure transducers. Thus the thermocouple is in direct contact with the oil film. An ice point was used for the reference junction and the output was displayed on a Hewlett Packard Model 3490A Multimeter. The thermocouple voltage output versus temperature agreed with standard copper-constantine calibration data.

The rotational speed of the eccentric shaft was measured by inputing the amplified signal from the magnetic transducer into a Monsanto Model 103A Counter Timer.

An overall view of the test rig and instrumentation is shown in Figure 6.

Method of Data Analysis

As discussed in the previous section, the output from the pressure transducer was displayed on the oscilloscope screen versus a time sweep. The time sweep was triggered when the eccentric lobe of the shaft was in the vertical up position. The distribution displayed on the screen was a voltage versus time curve. In order to get meaningful results this curve must first be converted to pressure versus angular rotation of the eccentric shaft and ultimately to pressure as a function of the squeeze film position angle θ.

In order to minimize the time required to obtain the data from the oscilloscope screen, and to increase the accuracy of the data recording process, a black and white picture of the distribution on the oscilloscope was taken using a 35 mm camera. After pictures were taken at all the desired locations of the outer cylinder the film was developed.

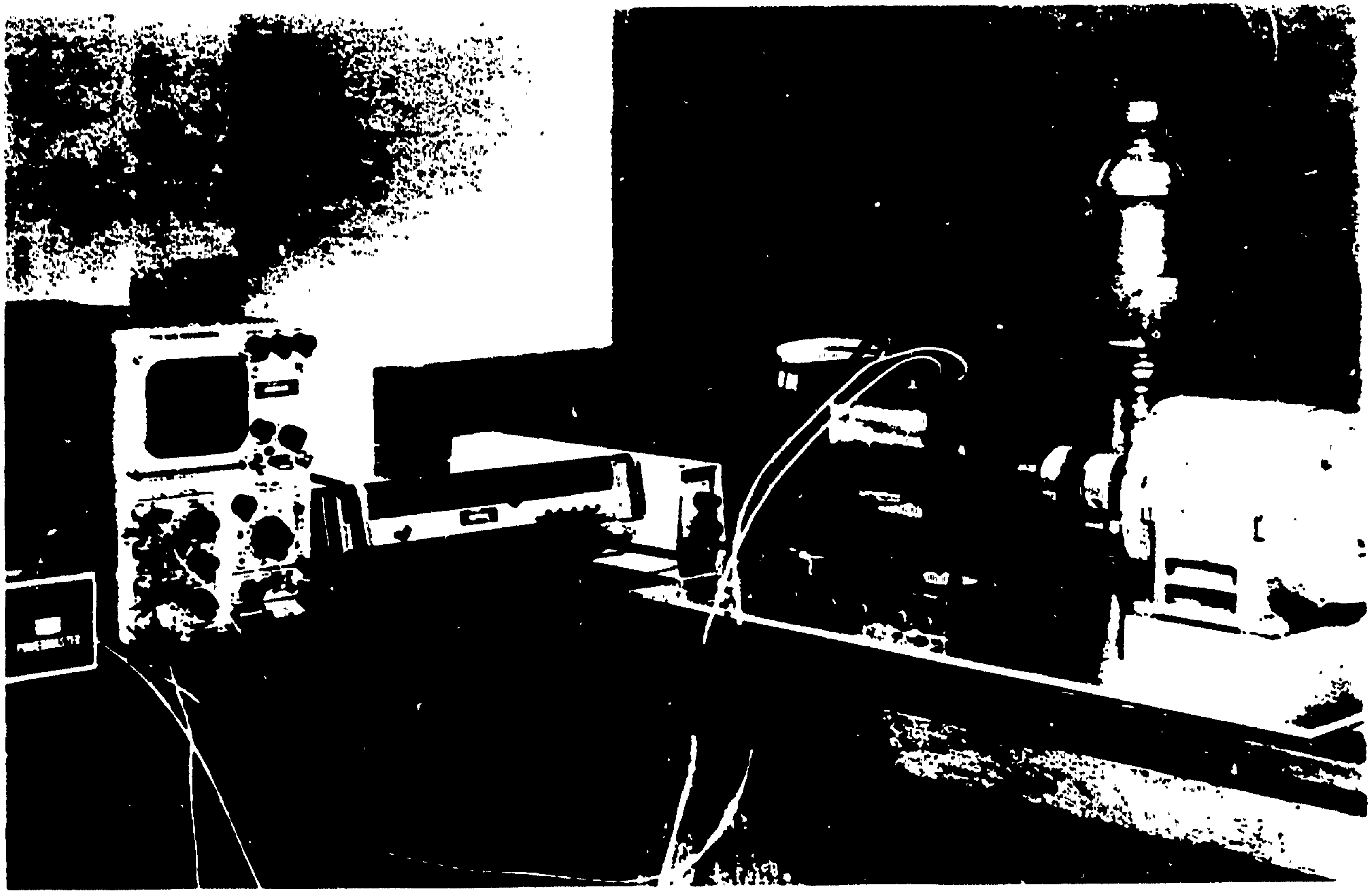

FIGURE 6. Photograph of Test Rig and Instrumentation

Reproduced from
best available copy.

The negatives were then cut and installed in plastic slides. These slides were put into a projector and displayed on a screen. The data were then recorded from the projection on the screen.

The time sweep of the oscilloscope was adjusted so that each full cycle of the curve covered thirty-six divisions on the oscilloscope screen. Thus each division represented ten degrees of shaft rotation.

The data obtained from the slide were the output from the pressure transducer, in millivolts, versus shaft rotation, with readings taken at ten degree intervals. The voltages were then converted to pressures using the transducer calibration curves. Thus pressure as a function of shaft rotation was known.

Experimental data were recorded for two cases: (1) the eccentric shaft centered in the outer housing and (2) the eccentric shaft offset from the center of the outer housing. Henceforth these two cases will be referred to as the centered orbit case and the offset orbit case.

For the centered orbit case the angle of shaft rotation may be related to $\overline{\Theta}$, where $\overline{\Theta}$ is the angle between the point of maximum film thickness and the pressure transducer, measured in the direction of shaft rotation. Figure 7 shows the geometric relationship needed to determine $\overline{\Theta}$ from the angular position of the eccentric shaft and outer housing. The pressure $p(\overline{\Theta})$ refers to the pressure recorded by the transducer as the eccentric shaft rotates which is not necessarily the same as $p(\Theta)$.

For the centered orbit case it is evident that the pressure distribution versus Θ should be independent of the position of the pressure transducer, provided there are no external or unknown effects.

For the offset orbit case there are several additional variables that affect the pressure distribution. For this case n, $\dot{n}$, and ω_c are no longer constants, but are functions of the angular position of the shaft. Data were taken at each of the 36 positions of the outer housing as it was rotated

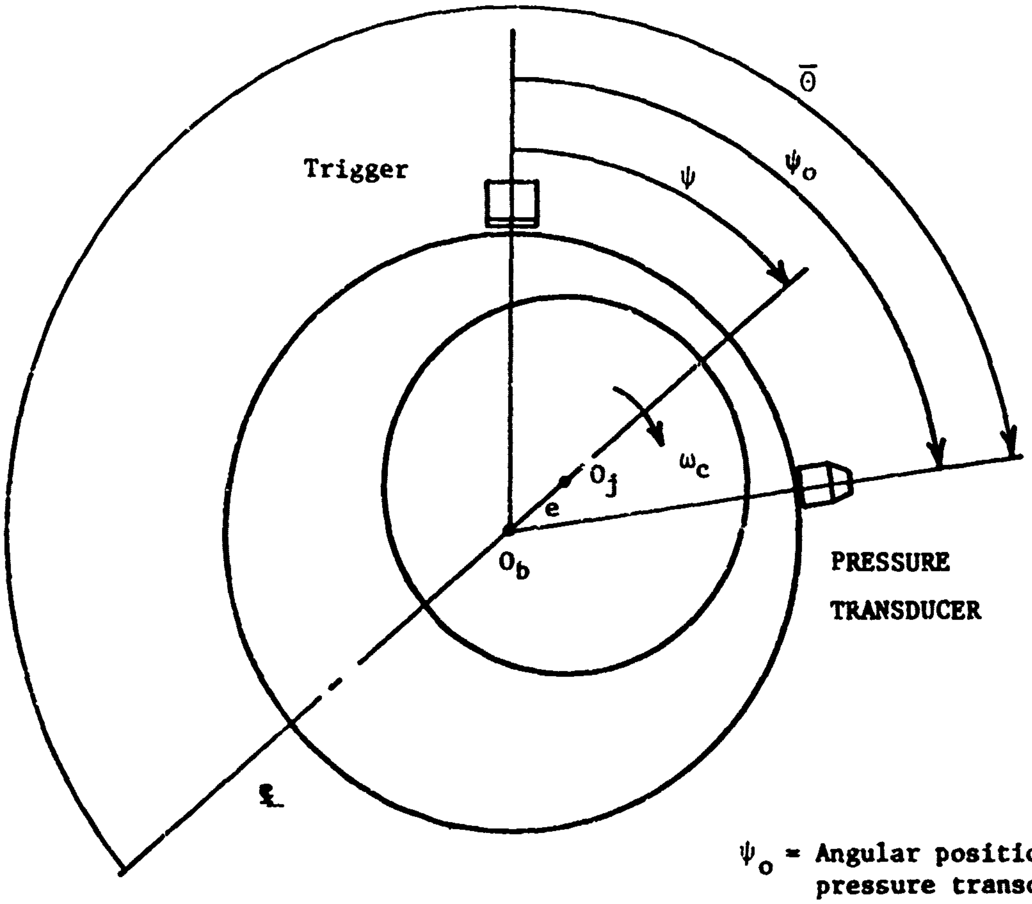
$\bar{\Theta}$
ψ_o
ψ
Trigger
ω_c
O_j
e
O_b
PRESSURE
TRANSDUCER
℄

ψ_o = Angular position of pressure transducer

ψ = Angle of eccentric shaft from vertical up position = $\omega_c t$

$$\bar{\Theta} = \pi + \psi_o - \psi$$

FIGURE 7. Geometric Relationship Between $\bar{\Theta}$ and the Angular Position of the Eccentric Shaft

through 360 degrees in 10 degree increments. In order to find the pressure distribution about the journal in one particular location, the pressure corresponding to that journal location must be obtained from each of the thirty-six photographs. For example, if it was desired that the pressure distribution about the journal be found when the eccentric lobe had rotated 180 degrees from the vertical up position, then the pressure corresponding to the eighteenth division of each of the photographs would be recorded. The angular relation between the journal position and the pressure transducer determines the value of θ for each of the readings.

The pressure distributions obtained for both cases were compared to the existing squeeze film theories. The pressure distributions were then numerically integrated to obtain the film force coefficients.

A description and listing of the computer program's used in the data analysis are given in Appendix IV.

Experimental Procedure

In order to facilitate the duplication of the data contained in this report and to aid future experimental studies using this test rig, a step by step procedure of the data taking process will be outlined.

1. Turn on all instrumentation two or three hours before taking data in order that they may become thermally stable.
2. Obtain ice and water in a thermos bottle for the thermocouple reference junction.
3. Check the oil supply in the holding tank.
4. Rotate the outer housing to bring the supply orifice to the top. Remove the supply hose and orifice. Fill the squeeze film clearance with oil from the holding tank while rotating the eccentric shaft by hand. Reinstall the orifice and supply line, making sure there is no air trapped in the supply line.
5. Adjust the pressure regulator of the compressed air supply to obtain the desired supply pressure.
6. Check the voltage output of the DC power source and adjust the rheostat to obtain 10.0 volts.
7. Set the oscilloscope time sweep to trigger on an external negative signal with a positive slope. Run the experimental rig and adjust the time sweep so that one pressure cycle covers 36 divisions on the oscilloscope. Adjust the sensitivity of the oscilloscope to get the desired amplitude of the transducer signal on the screen. Record the voltage/division setting.
8. After the rig has been still for 3 to 5 minutes record the supply pressure as shown by the oscilloscope.

9. Using a 35 mm camera and ASA 400 film, the shutter speed should be set at 1/15 second and the f-stop set at between 2.8 and 4.0.
10. Rotate the outer cylinder to the desired location and install the locking pin. Run the rig until the desired oil film temperature is reached as determined by the output of the thermocouple. A picture is then taken of the oscilloscope screeen and a record is made of the picture number, outer cylinder location and thermocouple output.
11. The outer cylinder is then rotated to another location and step 10 is repeated making sure that all pictures are taken at the same oil film temperature.

RESULTS AND DISCUSSION

Problems with the experimental apparatus prevented this study from being as extensive as had been intended from the onset. Much of the effort was directed toward redesign of the test rig to prevent conditions not associated with squeeze film flow from altering the pressure distribution about the orbiting journal. These problems only point to the difficulty in trying to describe squeeze film bearing damper operation under actual conditions, where the damper is interacting with the dynamics of the rotor-bearing-support system. During actual operation the external conditions which can alter the squeeze film are more prevalent and much more difficult to control.

In spite of the problems which occurred during this study, valuable insight was gained into the nature of the hydrodynamics of the squeeze film.

Problems with the Experimental Rig

For the centered orbit case, the journal orbits about the center of the outer housing with a radius equal to the shaft eccentricity. Due to symmetry, the pressure distribution with respect to $\overline{\theta}$ should be independent of the position of the outer housing and pressure transducer. During the initial running of the rig it became evident that the pressure distribution was changing as the outer housing was rotated. Because there was no apparent explanation for these changes, a fairly extensive period of trouble shooting and redesign was initiated to determine the cause of the changes and to modify the test rig accordingly. The following is a discussion of some of the problems encountered in the rig and a description of the modifications carried out to correct them.

During each pressure cycle, high frequency pressure fluctuations of large amplitude were observed, superimposed on the pressure distribution displayed on the oscilloscope screen. These pressure fluctuations had a shape resembling an amplitude-time plot of the damped, free vibration of a spring-mass system. A large radial pin was being used to prevent relative rotation between the journal and the outer housing. Due to the shape of the pressure fluctuations it was believed that they were caused by the journal and shaft vibrating due to impact with the stiff radial pin. The radial pin was therefore removed and four, small axial pins were used to constrain the journal. The axial pins were designed to bend under loads, thus reducing the impact forces on the journal.

A belt drive had been used between the electric motor and the eccentric shaft. Misalignment between the belt pulleys resulted in an axial load on the eccentric shaft and journal. The axial positioning of the journal was controlled by the compression of the o'rings used in sealing the ends of the journal. An axial load on the journal therefore results in expansion and contraction of the o'rings which could cause a volumetric change within the squeeze film, resulting in pressure fluctuations. The belt drive was replaced by a flexible coupling designed to be unable to transmit axial loads between the motor and eccentric shaft.

It had also been observed that the inlet conditions had a significant effect upon the pressure distribution measured by the pressure transducer. The pressure distribution could be altered by varying the length of the supply hose or by restricting the hose in any way. In order to get meaningful, repeatable results it was felt necessary to make the pressure distribution independent of the supply hose and tank, except for the magnitude of the supply pressure. Initially a .110 inch diameter inlet was used in the outer housing to supply oil to the squeeze film clearance. An orifice was designed to be installed in the inlet. It was desired that the orifice design be such that the supply pressure would be maintained in the squeeze film, but that the pressure distribution would not be altered during a pressure cycle by flow through the inlet. Experimentation with several different designs resulted in an orifice with a 1/64 inch diameter hole, two inches long.

The o'ring grooves at each end of the journal were redesigned so that the o'rings were a snug fit in the grooves. This was done to ensure that the o'rings could not move in the grooves causing a volumetric change in the squeeze film clearance.

Measurements were made of various parts of the disassembled rig to determine if they were machined to drawing specifications. Special care was taken in measuring the eccentric shaft and outer housing supports, as they control the relative position of the journal within the housing. The rig was reassembled and the eccentricity of the journal was measured through the holes provided for the pressure transducers. These measurements indicated that the outer housing and eccentric shaft were concentric within .0005 inch.

These modifications resulted in a large improvement in the observed pressure distributions. The large, high frequency pressure fluctuations during each cycle were no longer present and the pressure distribution appeared to be independent of the supply hose and tank. Changes still occurred in the pressure distribution as the outer cylinder was rotated but not to the extent seen previously. The cause of these changes is not known but may be attributed to some type of volumetric change of the squeeze film clearance or a change in the squeeze film geometry due to dynamic loads on the rolling element bearings and supports.

Centered Orbit Case

As discussed in the previous section, some changes still occurred in the pressure distribution as the outer cylinder and pressure transducer were rotated. Due to these changes, data is presented for four perpendicular positions of the outer cylinder. The angular location of the pressure transducer for these positions is 0, 90, 180 and 270 degrees from the vertical up position, in the direction of shaft rotation.

Data were recorded using both SAE 10 and SAE 50 oil. In order to facilitate comparison with the existing theory the results were put into the non-dimensional form:

$$\frac{p - p_o}{\mu r_j^2 \omega_c / c^2}$$

The results are shown in comparison to the "long bearing" and "short bearing" theory in Figures 8, 9, 10 and 11 for the SAE 10 oil and in Figures 12, 13, 14 and 15 for the SAE 50 oil.

The general shape of the experimental curves follow the "long bearing"

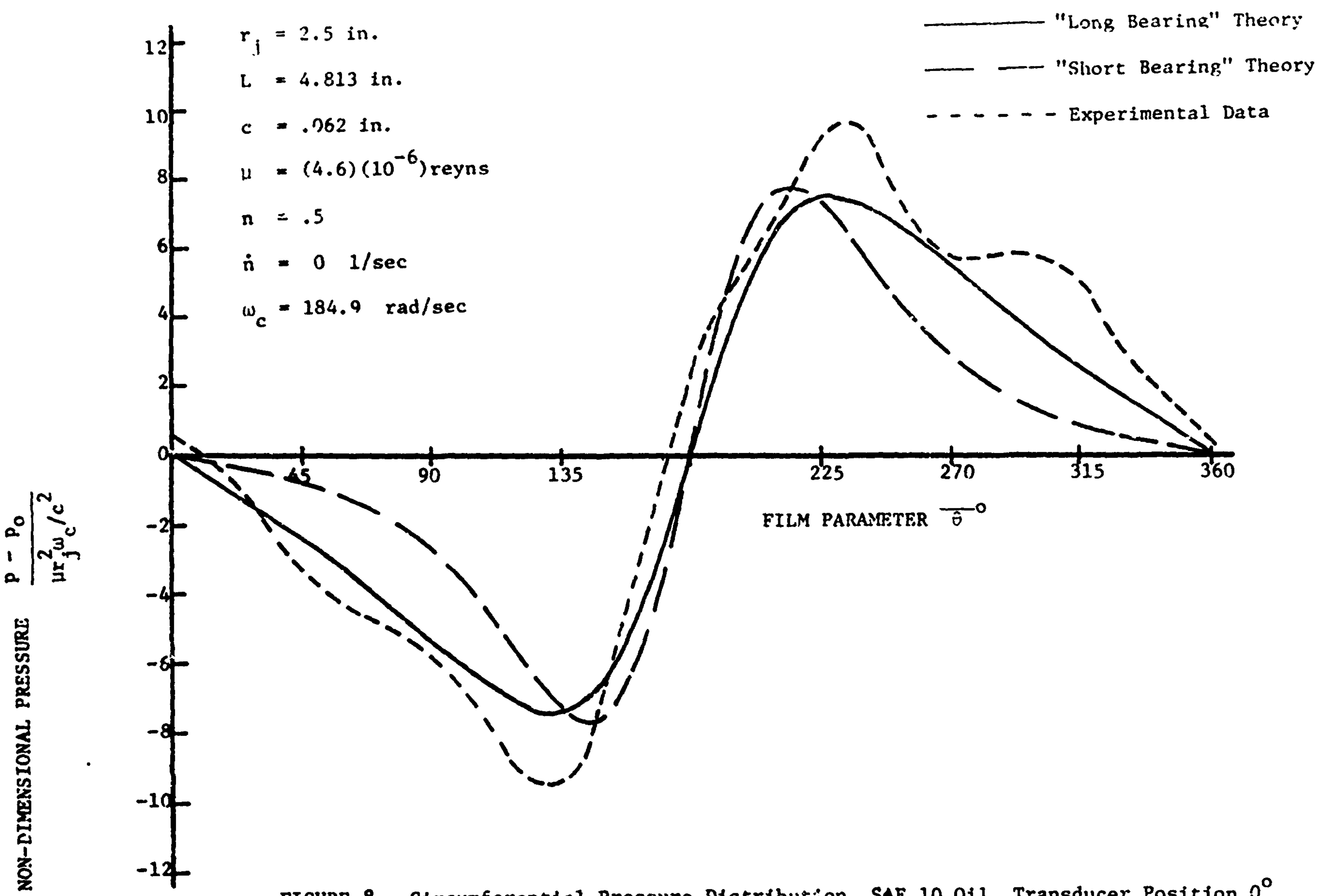

FIGURE 8 - Circumferential Pressure Distribution, SAE 10 Oil, Transducer Position 0°

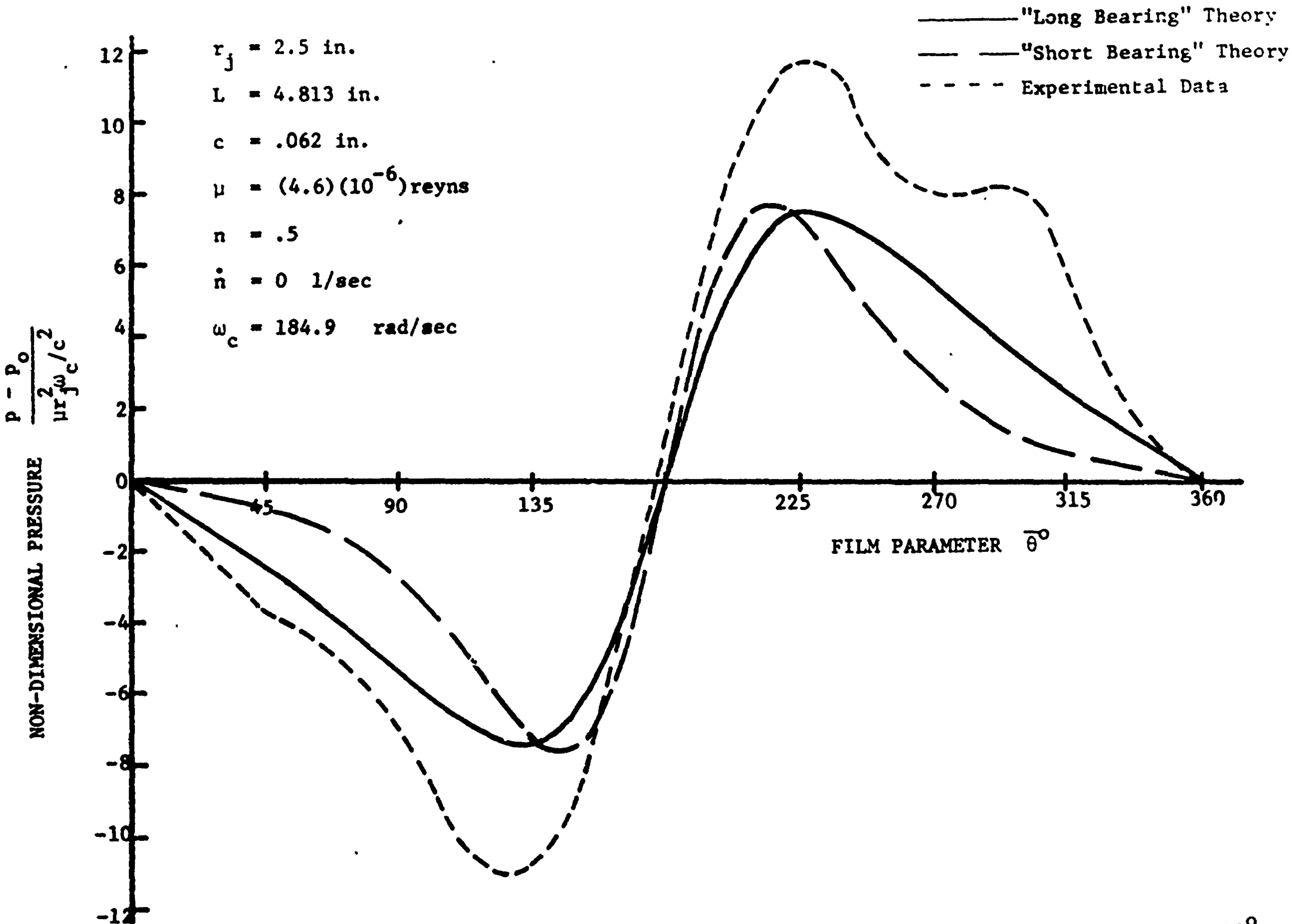

FIGURE 9 - Circumferential Pressure Distribution, SAE 10 oil, Transducer Position 90°

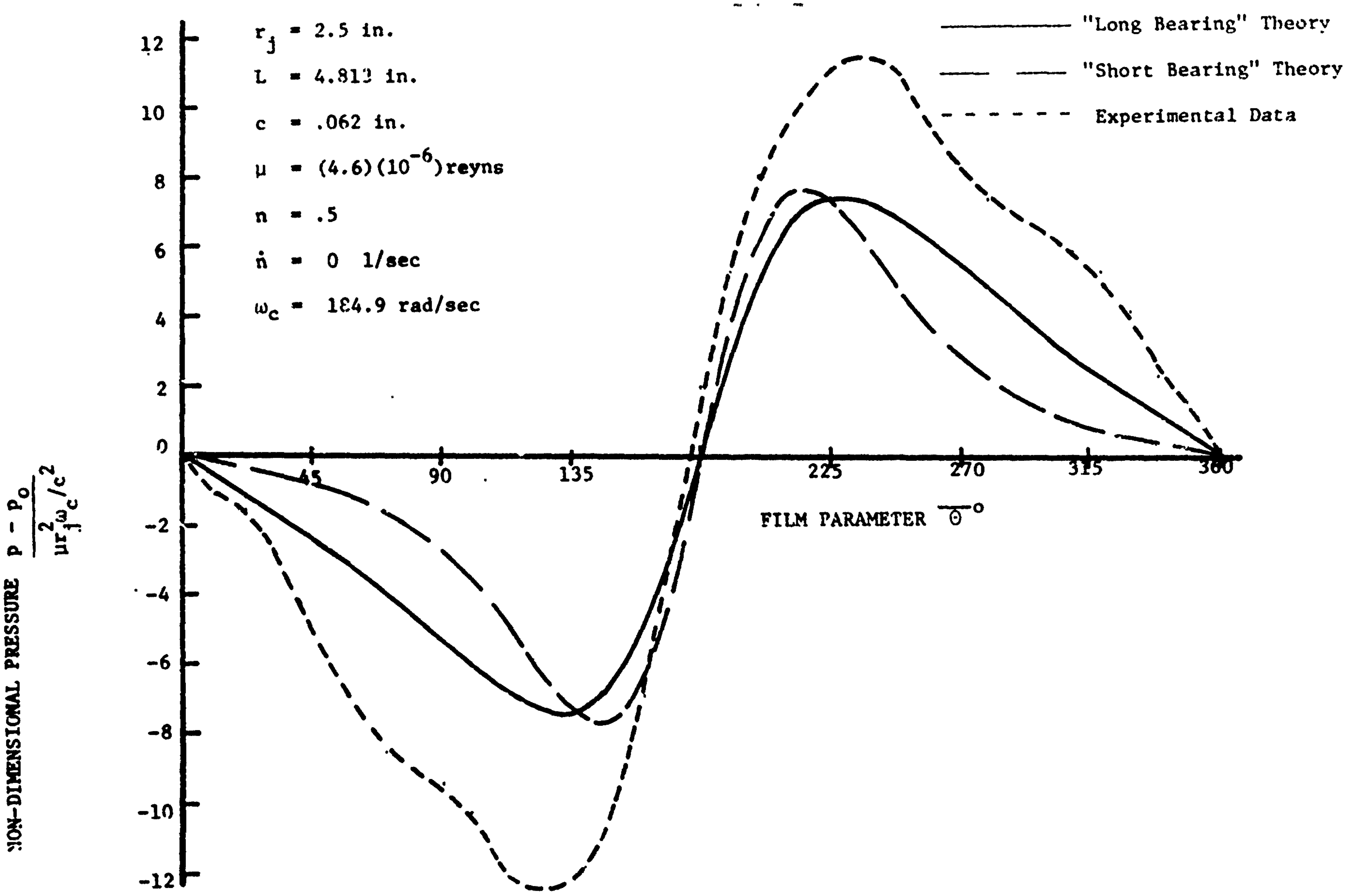

FIGURE 10 - Circumferential Pressure Distribution,-SAE 10 Oil, Transducer Position 180°

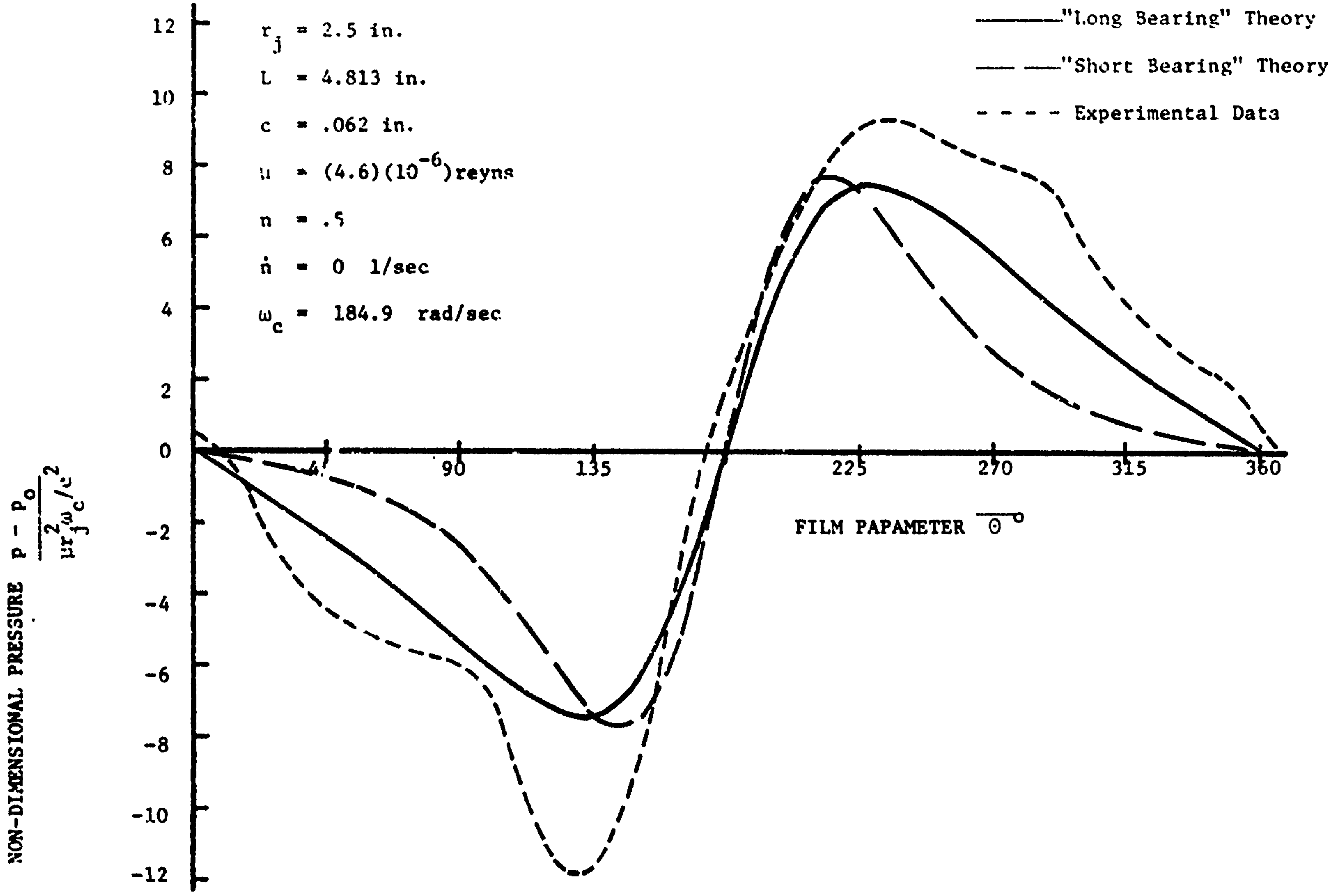

FIGURE 11 - Circumferential Pressure Distribution, SAE 10 Oil, Transducer Position 270°

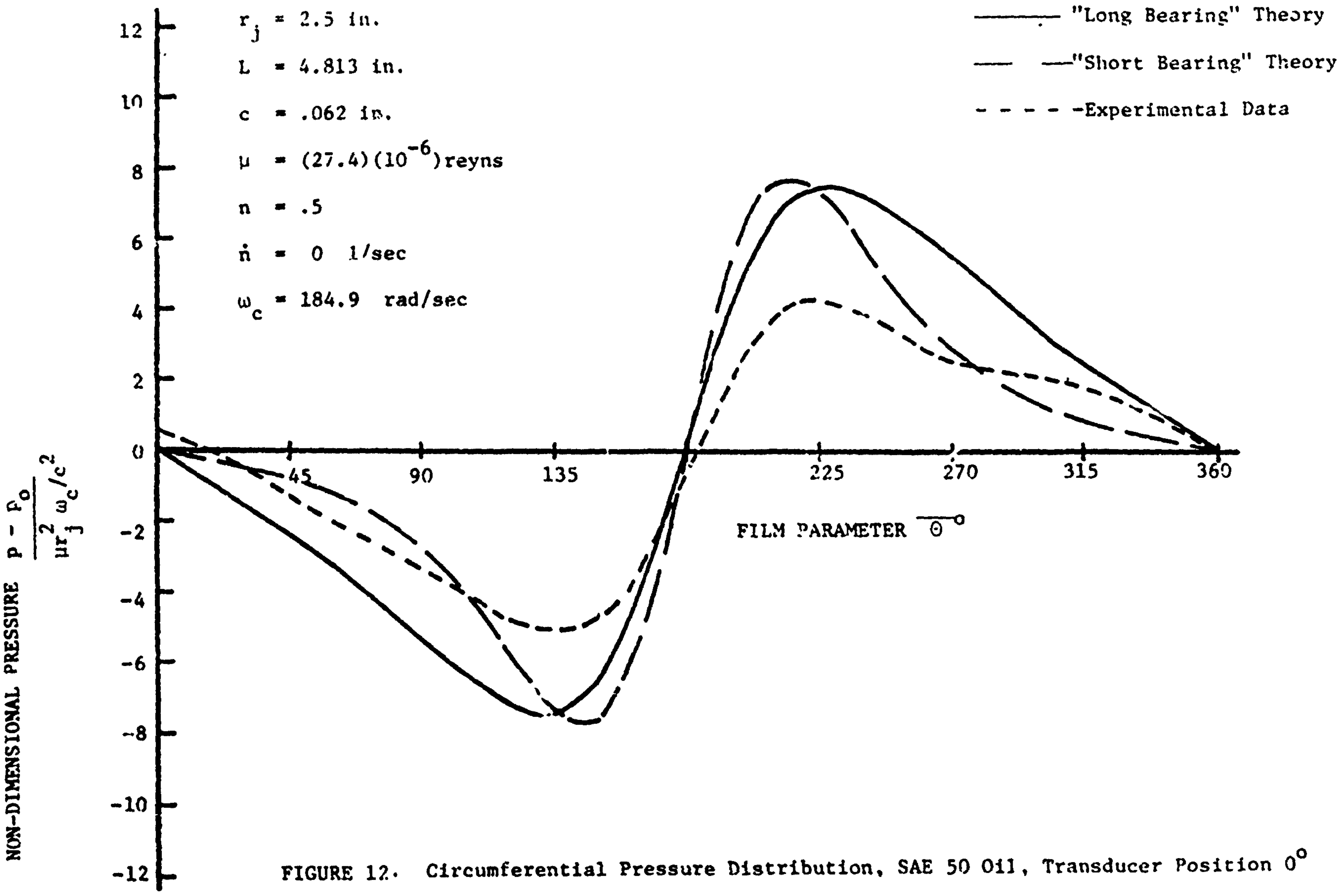

FIGURE 12. Circumferential Pressure Distribution, SAE 50 Oil, Transducer Position 0°

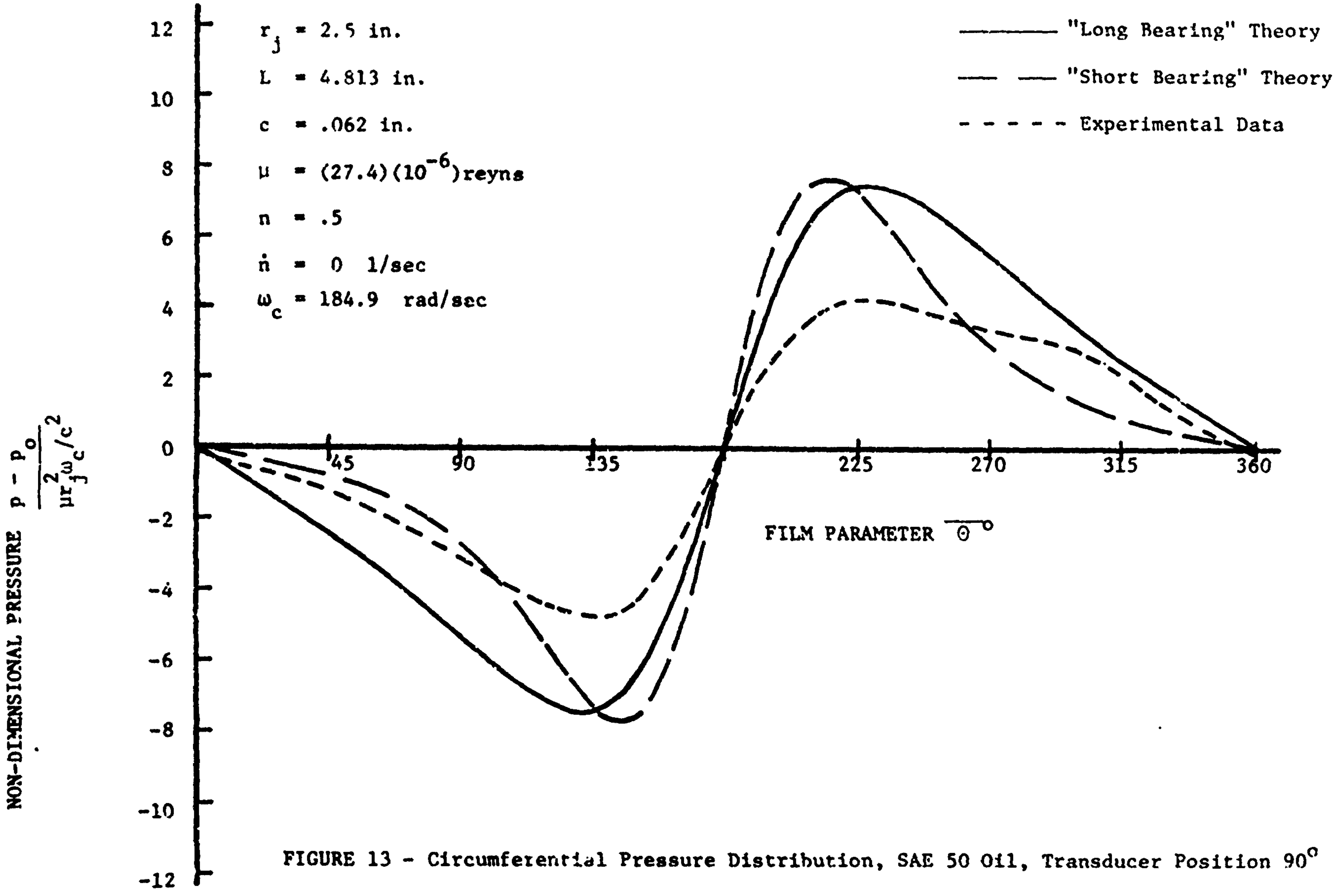

FIGURE 13 - Circumferential Pressure Distribution, SAE 50 Oil, Transducer Position 90°

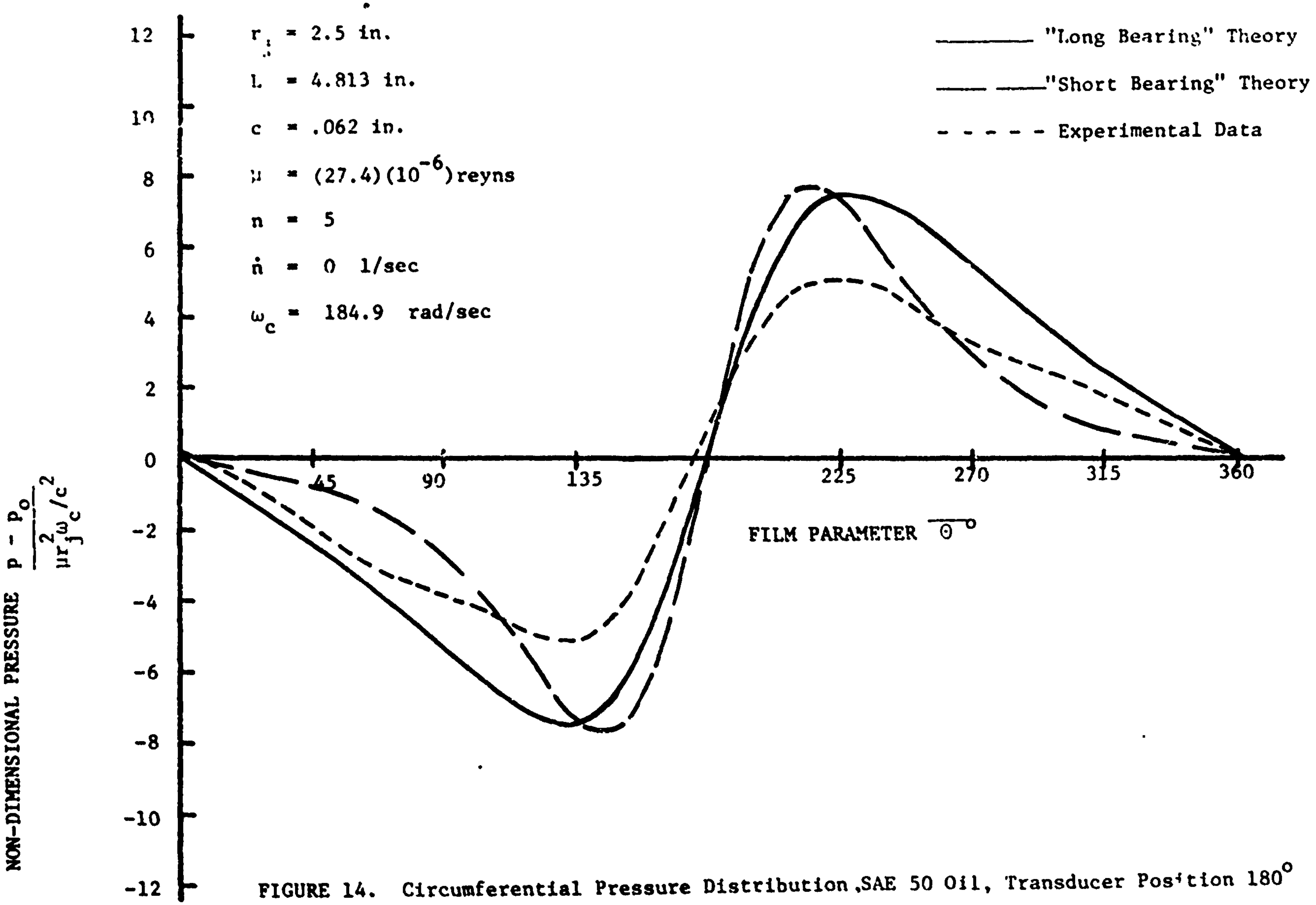

FIGURE 14. Circumferential Pressure Distribution, SAE 50 Oil, Transducer Position 180°

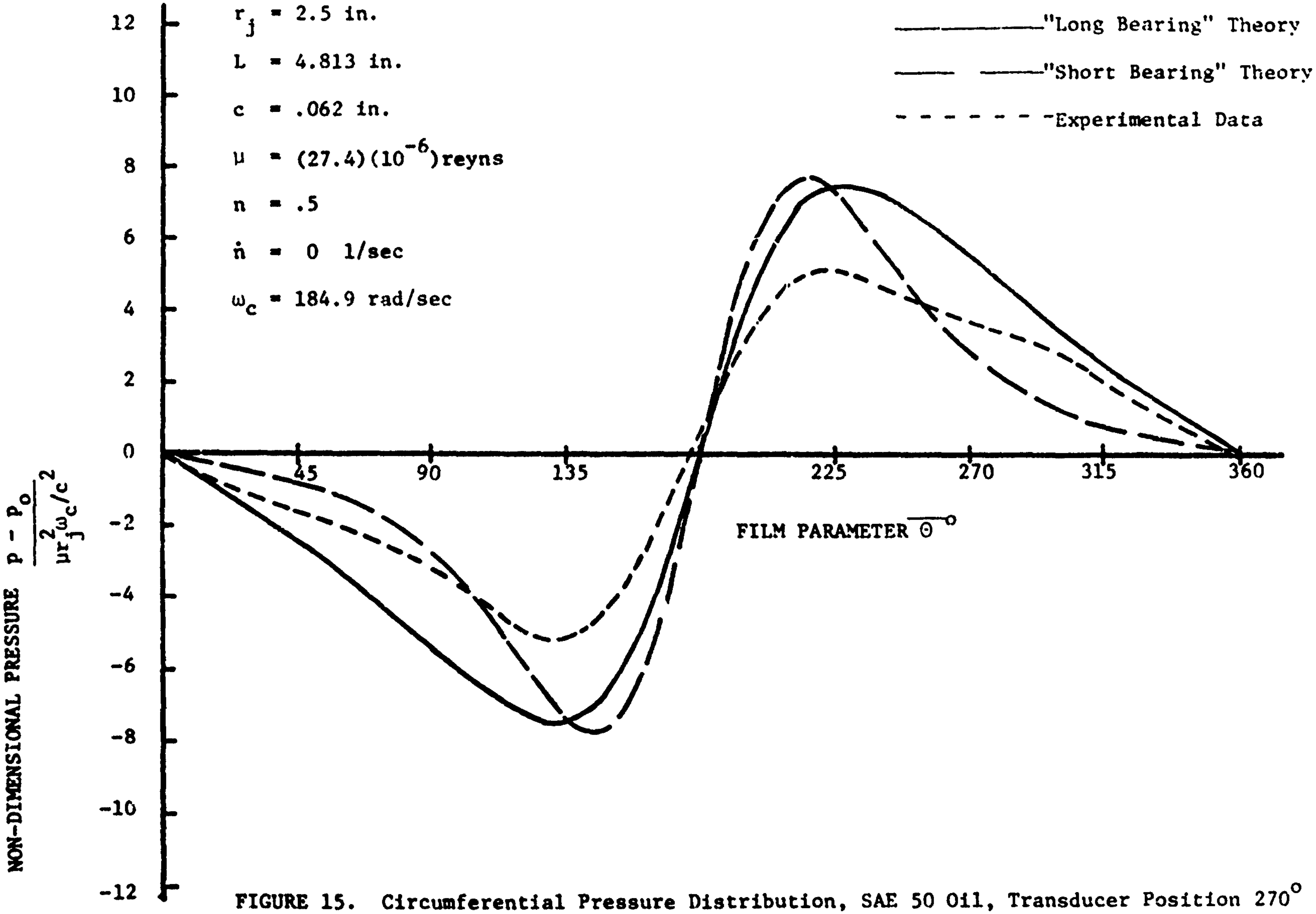

FIGURE 15. Circumferential Pressure Distribution, SAE 50 Oil, Transducer Position 270°

theory with fairly good agreement. The peak positive and peak negative pressures occur at the predicted values of 0. However, there is a large variation in the amplitudes of the pressures, with the SAE 10 oil producing peak to peak pressures 53% greater than predicted while the SAE 50 oil produced peak to peak pressures 33% less than predicted.

Thus the measured data deviates from the linear dependence on viscosity as predicted by Reynolds' equation.

Since Reynolds' equation is based on an assumption of laminar flow, one possible explanation is suggested by Vohr's [8] study of flow between non-concentric rotating cylinders. In this investigation the nature of Taylor vortex flow and turbulence was studied. It was shown that after the transition from laminar flow to vortex flow the shape of the resulting pressure distributions is nearly unchanged while the peak to peak pressures are significantly larger than predicted by the "long bearing" theory. Criteria for the onset of Taylor vortices were developed using a modified Taylor number:

$$\sqrt{1/2\ T_{cr.}} = 41.2, \quad \sqrt{1/2\ T_{cr.}} = \frac{Vc\rho}{\mu}\sqrt{\frac{c}{r_j}} = Re\sqrt{\frac{c}{r_j}}$$

For journal bearings, the velocity V was defined as the surface velocity of the journal:

$$V = r_j\omega_j$$

In squeeze film dampers the rotation of the line of centers (ω_c) produces the viscous pressure distribution defined by Reynolds' equation in a rotating coordinate system. Since the Reynolds' number represents the dimensionless ratio of inertia forces to viscous shear forces, there is a question as to what value of V is appropriate to use in predicting flow transition for this case. Although no experimental data exists to verify transition values for the case of a rotating line of centers, an argument can be made for using:

$$V = r_j \omega_c$$

This definition for V results in a value of 80.2 for the SAE 10 oil and a value of 14.0 for the SAE 50 oil. This indicates that the higher than predicted pressures are due to a transition from laminar to vortex flow.

The pressure data was numerically integrated to obtain the radial and tangential force components, and also the damping coefficient B given by Reference 6. An explanation and listing of the program used to accomplish this is given in Appendix 4. The force components for the SAE 10 and the SAE 50 oil, the damping coefficient B, and the values predicted using the "long bearing" theory are presented in Table 2. As expected from the pressure distributions, the SAE 10 oil had values approximately 35% greater than predicted, while the SAE 50 oil had values approximately 36% less than predicted by the "long bearing" theory. Thomsen and Anderson [6], in their experimental study, found that the damping coefficient was significantly larger than predicted by the theory when they used light oil (6 centipoise) and large clearances in their test apparatus. It is under these conditions that the transition from laminar to vortex flow would be expected to occur. Using the criteria given above and the data given by Thomsen and Anderson a value of 59.4 is obtained for the transition parameter. Thus it may be surmised that the larger than predicted damping coefficient was obtained due to a transition from laminar to vortex flow. Although there is no conclusive experimental evidence,experience in industry has indicated that there may not be the linear relationship between the force components and viscosity as predicted by the laminar theory. A possible explanation is that the dampers may be operating in the vortex or turbulent flow regime where the force components are not linearly dependent on the viscosity.

TYPE OF LUBRICANT	OUTER HOUSING POSITION (degrees)	EXPERIMENTAL DATA			"LONG BEARING" THEORY		
		Tangential (lbf)	Radial (lbf)	B (lbf-sec/in)	Tangential (lbf)	Radial (lbf)	B (lbf-sec/in)
SAE 10 $\mu = (4.6)(10^{-6})$ reyns	0	405.0	6.9	70.6	330.1	0.0	57.6
	90	503.7	10.8	87.9			
	180	563.7	-2.3	98.3			
	270	463.8	-9.7	80.8			
SAE 50 $\mu = (27.4)(10^{-6})$ reyns	0°	1162.3	-161.5	204.7	1964.5	0.0	339.3
	90	1208.1	-57.5	210.7			
	180	1329.2	75.7	231.8			
	270	1300.6	28.7	226.9			

$n = .5$
$\dot{n} = 0$ 1/sec
$c = .062$ in.
$\omega_c = 184.9$ rad/sec
$r_j = 2.5$ in.
$L = 4.813$ in.
$B = \frac{F_x}{e\omega_c}$

TABLE 2: FORCE COMPONENTS FOR CENTERED ORBIT CASE

A calculation of the Reynolds number for the damper in a recently developed high speed turboshaft engine yields a value of about 2500, indicating turbulent flow. Engines with more moderate shaft speeds may have dampers operating in either the vortex or laminar flow regime. Thus, a determination of the proper flow regime appears to be an important prerequisite to an accurate prediction of the dynamic force response for engine dampers.

The deviation of the results for the SAE 10 oil from the "long bearing" theory may be explained by a transition from laminar to vortex flow. However, this is not true for the SAE 50 oil. The SAE 50 oil produced peak to peak pressures 33% less than predicted by the "long bearing" theory and force components 36% less than predicted by the "long bearing" theory. The deviation is perhaps not surprising due to the differences in the boundary conditions of the theory and the test rig. As discussed previously, the inlet of the test rig does not meet the boundary condition imposed by the theory. However, with the 1/64 inch orifice it is believed that the inlet flow cannot dynamically follow the changing pressures experienced by the inlet and that the pressure at $\Theta = 0$ stabilizes to some constant pressure.

The use of end seals results in another deviation from the boundary conditions for Reynolds' theory. End seals prevent axial flow, consistent with the "long bearing" theory, but impose the condition of zero fluid velocity at the ends. This is a possible explanation for the lower pressures produced using the SAE 50 oil.

Observations with pressure transducers located away from the central plane of the outer housing indicated that peak to peak pressures did not vary in the axial direction, but that there was approximately a 10% drop of p_0 from the center, toward the end of the journal. These results are reasonably consistent with the "long bearing" theory which predicts negligible pressure variation in the axial direction.

Effect of the Inlet Conditions

In the initial running of the test rig it was observed that the inlet conditions altered the pressure distribution as recorded by the pressure transducer. In order to minimize the inlet effects the 1/64 inch orifice was installed in the inlet for the above tests.

It was then decided to study the effect of a relatively unrestricted inlet. The orifice was removed leaving the .110 inch supply hole. The tests were run using SAE 10 oil and data were recorded for two perpendicular positions of the pressure transducer. The results are shown in comparison to the "long bearing" theory in Figures 16 and 17. It should be emphasized that these data do not represent the instantaneous pressure distribution about the journal, but are the pressures recorded by the pressure transducer as the eccentric shaft rotates.

With the SAE 10 oil and the .110 inch supply hole the flow through the inlet is relatively unrestricted. Thus the pressure of the squeeze film at the location of the inlet remains at the supply pressure. As the eccentric shaft rotates, the position of the inlet with respect to θ is constantly changing. If it is assumed that the Sommerfeld distribution is still valid then the value of p_o must be constantly changing in order that $p(\theta)$ at the inlet equals the supply pressure. Thus the instantaneous pressure distribution about the journal would be given by the Sommerfeld theory with the value of p_o such that the pressure at the inlet equals the supply pressure. Figure 18 shows the effect of this condition.

Under the above assumptions a simplified theory was developed to predict the pressure distribution as recorded by the pressure transducer. The supply pressure for both the restricted and the unrestricted case was 45 psig. Using the data from the restricted case the quantity $[45 - p(\overline{\theta}_I)]$ was calculated

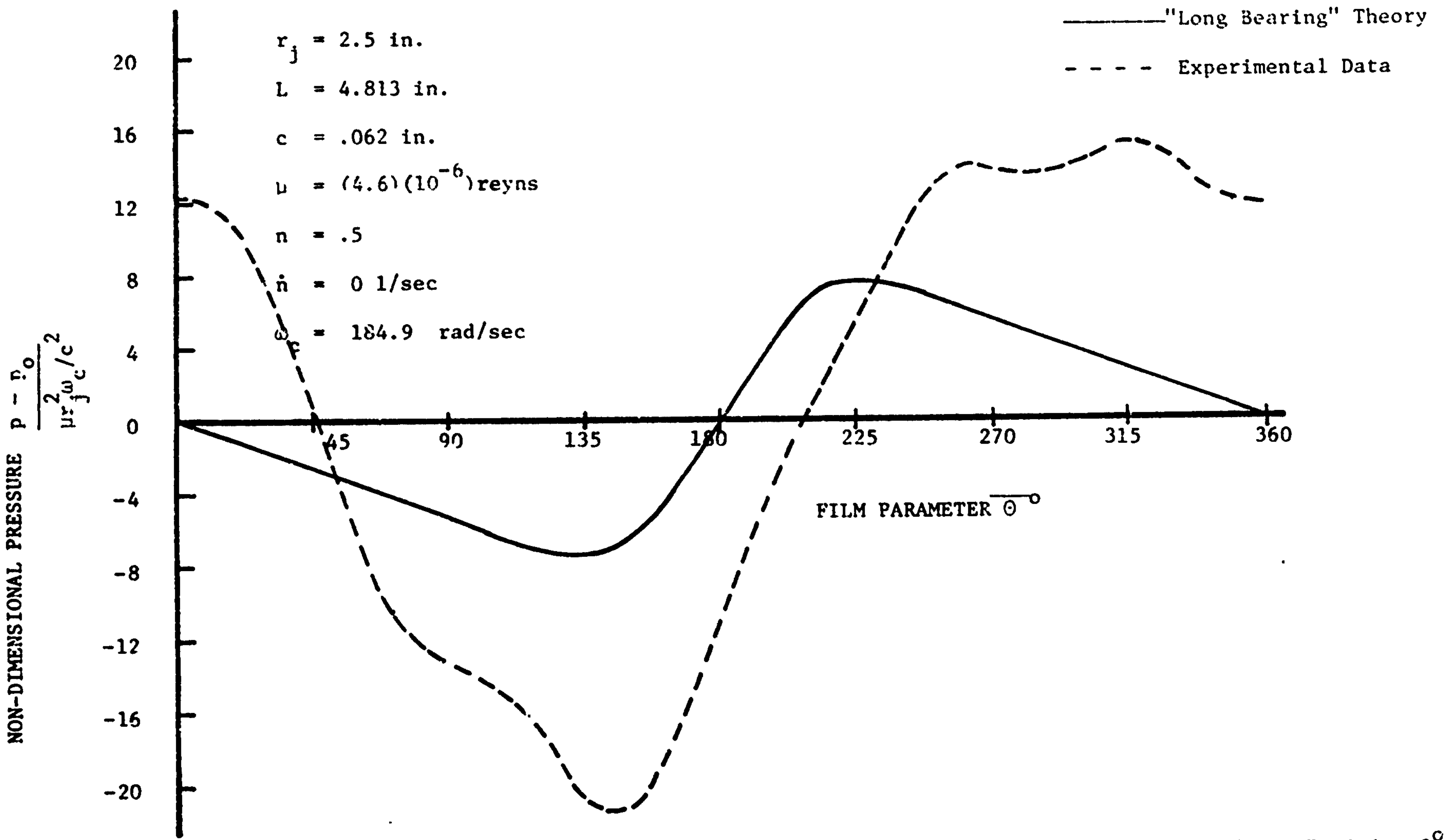

FIGURE 16. Circumferential Pressure Distribution, Unrestricted Inlet, Transducer Position 0°

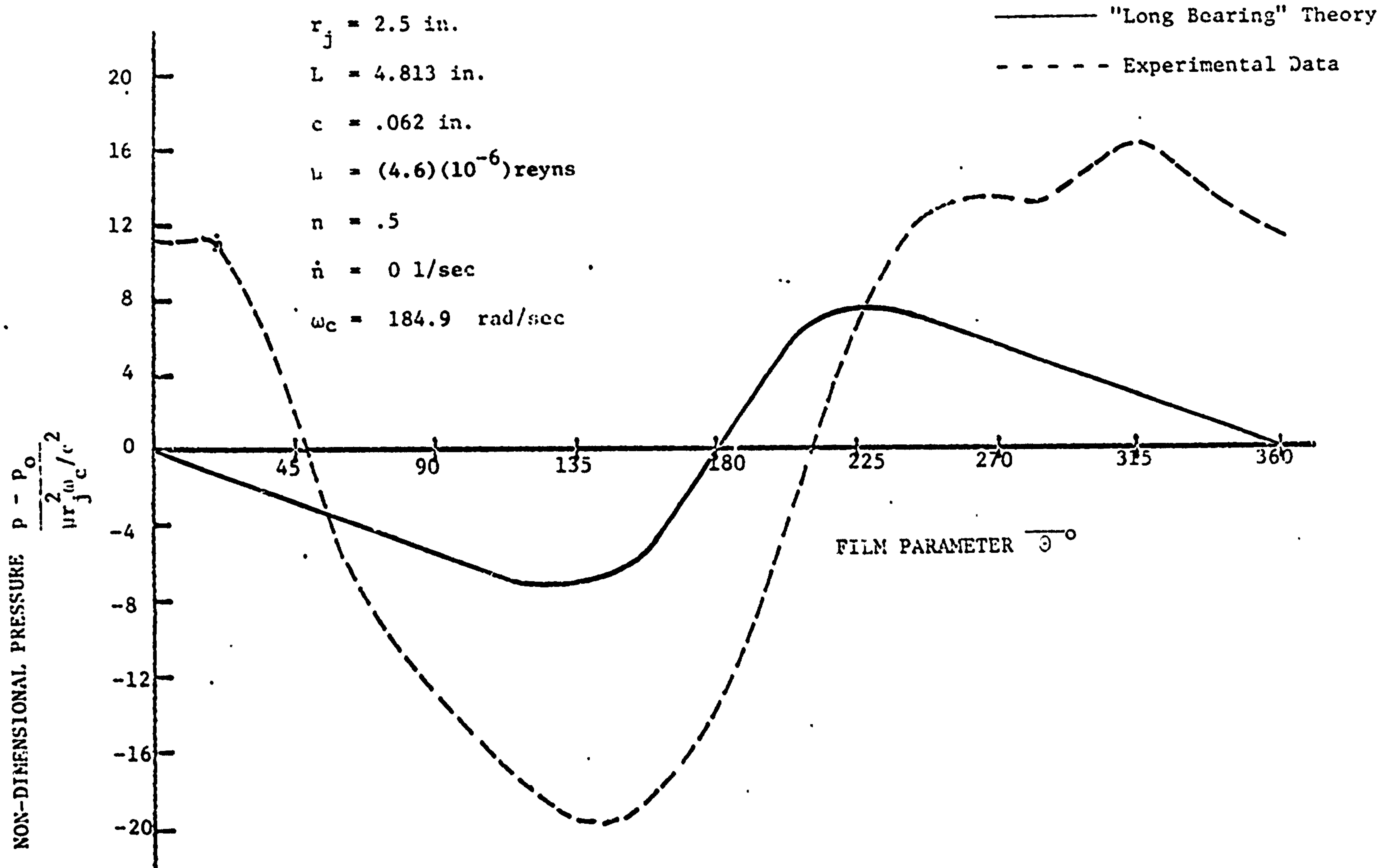

FIGURE 17. Circumferential Pressure Distribution, Unrestricted Inlet, Transducer Position 180°

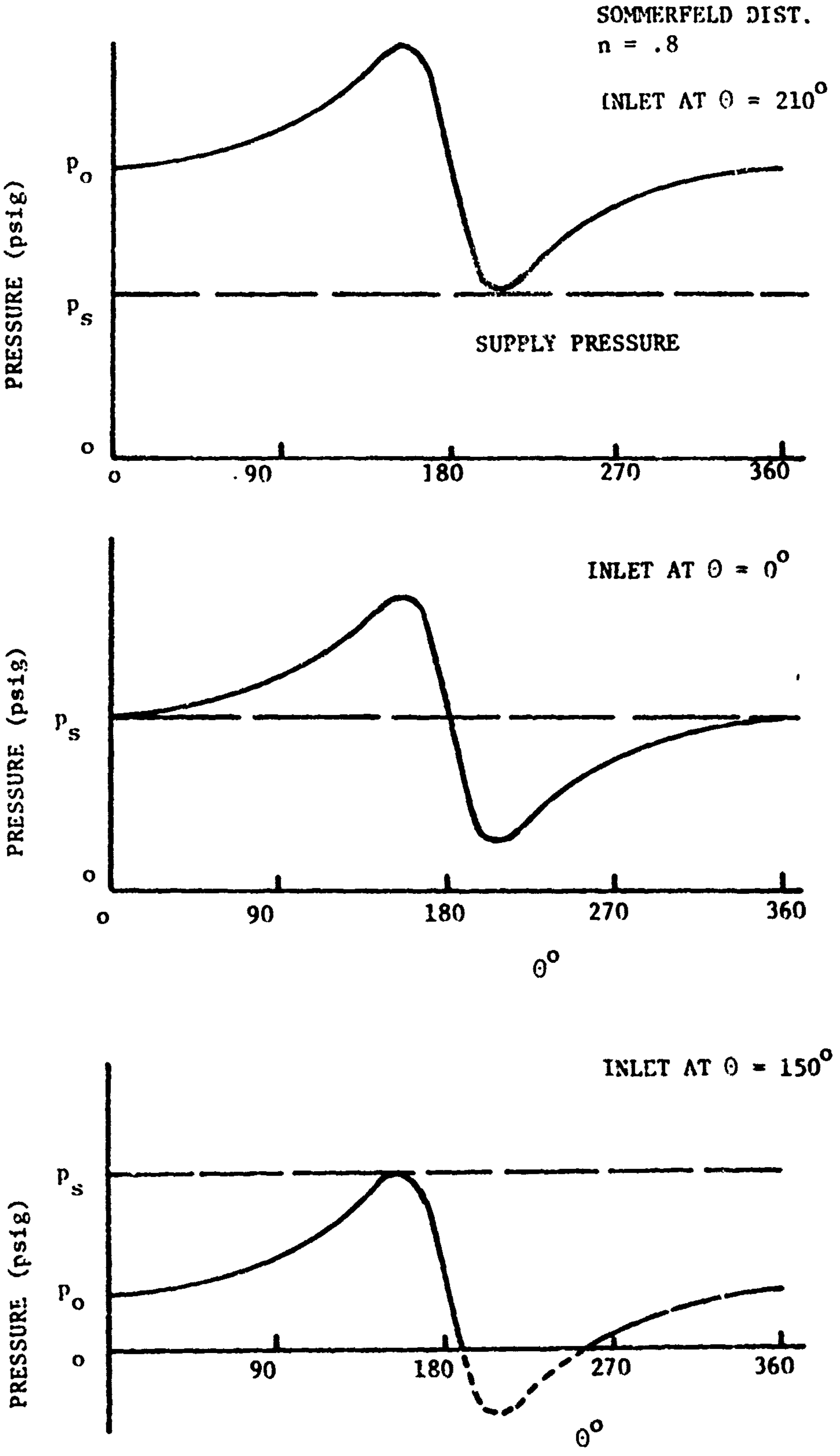

FIGURE 18. Effect of Unrestricted Inlet on "Long Bearing" Solution to Reynolds' Equation

at ten degree increments of $\overline{\theta}_I$, where $\overline{\theta}_I$ is the inlet position (see Figure 19). The quantity $[45 - p(\overline{\theta}_I)]$ represents the amount which $p(\overline{\theta})$ must be adjusted to predict the pressure distribution for an unrestricted inlet.

$$p(\overline{\theta}) \text{ unrestricted} = p(\overline{\theta}) \text{ restricted} + [45 - p(\overline{\theta}_I) \text{ restricted}]$$

The resulting curves are shown with the experimental results in Figures 20 and 21.

As can be seen from the figures there is good agreement between the shapes of the curves resulting from the simplified theory and the experimental results. It is evident, however, that the inlet is not unrestricted and that the inertia of the fluid is not negligible. It is most probably these effects which cause the phase and amplitude differences between the theory and the experimental results.

This would indicate that the simplified theory, and the assumptions upon which it is based are essentially correct. A radial inlet in an actual squeeze film damper design would probably fall between the restricted and unrestricted inlets studied in this investigation. However, the cyclic variation of the pressure distribution, as shown in Figure 18, would be present to some extent, with a resulting variation of the force components. If the supply pressure is small compared to the peak positive and peak negative pressures, as is true for actual squeeze film dampers, then the extent of the cavitated film region will vary throughout each cycle. This may result in the film being completely cavitated over portions of each cycle, resulting in a cyclic loss of the load carrying ability of the squeeze film.

Offset Orbit Case

The eccentric shaft was offset from the center of the outer housing by installing shims under the eccentric shaft supports. In this way the

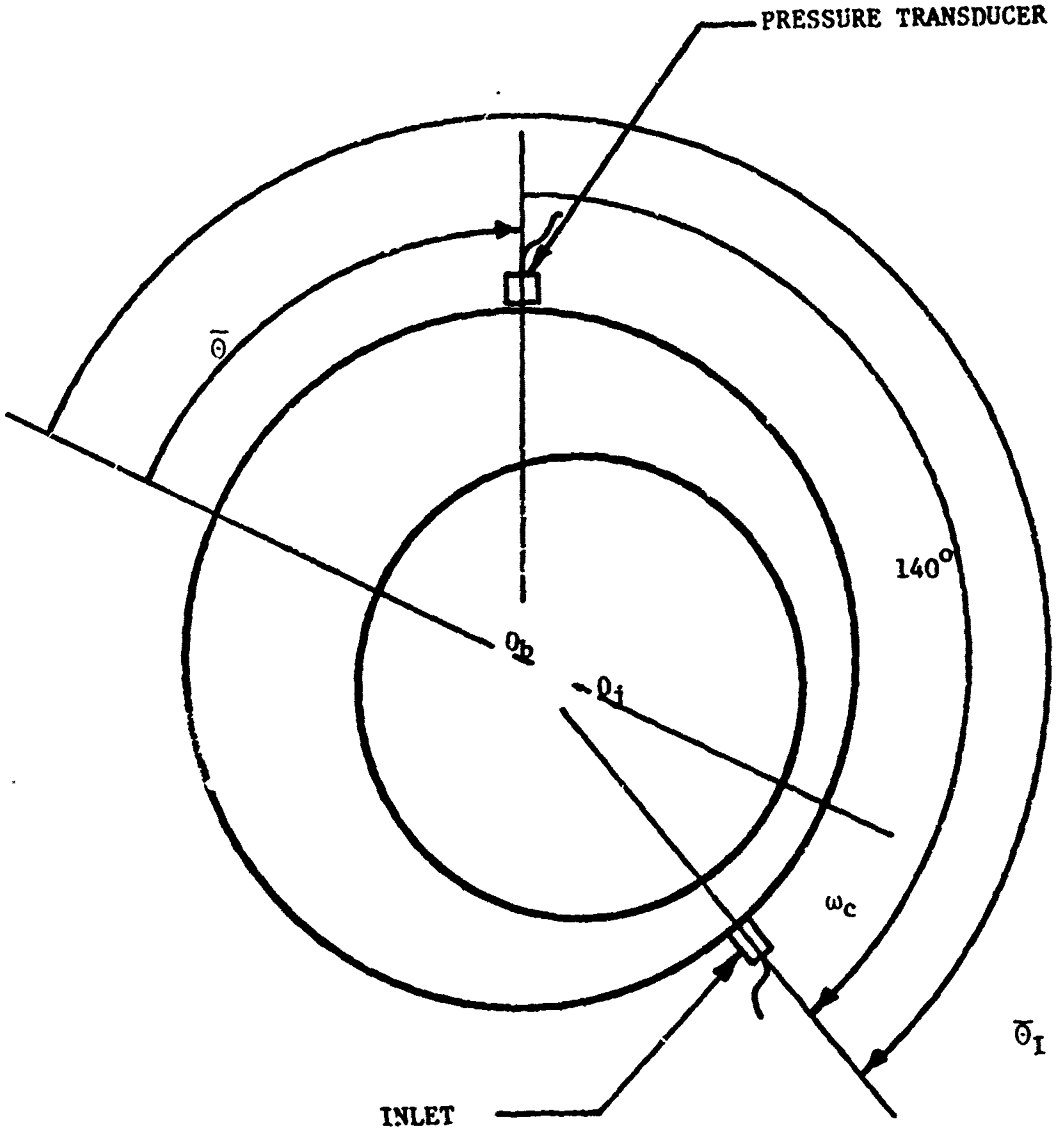
PRESSURE TRANSDUCER
$\bar{\Theta}$
140°
0_b
0_i
ω_c
$\bar{\Theta}_I$
INLET

$$\bar{\Theta}_I = \bar{\Theta} + 140^\circ$$

FIGURE 19. Angular Relationship Between the Pressure Transducer and Inlet

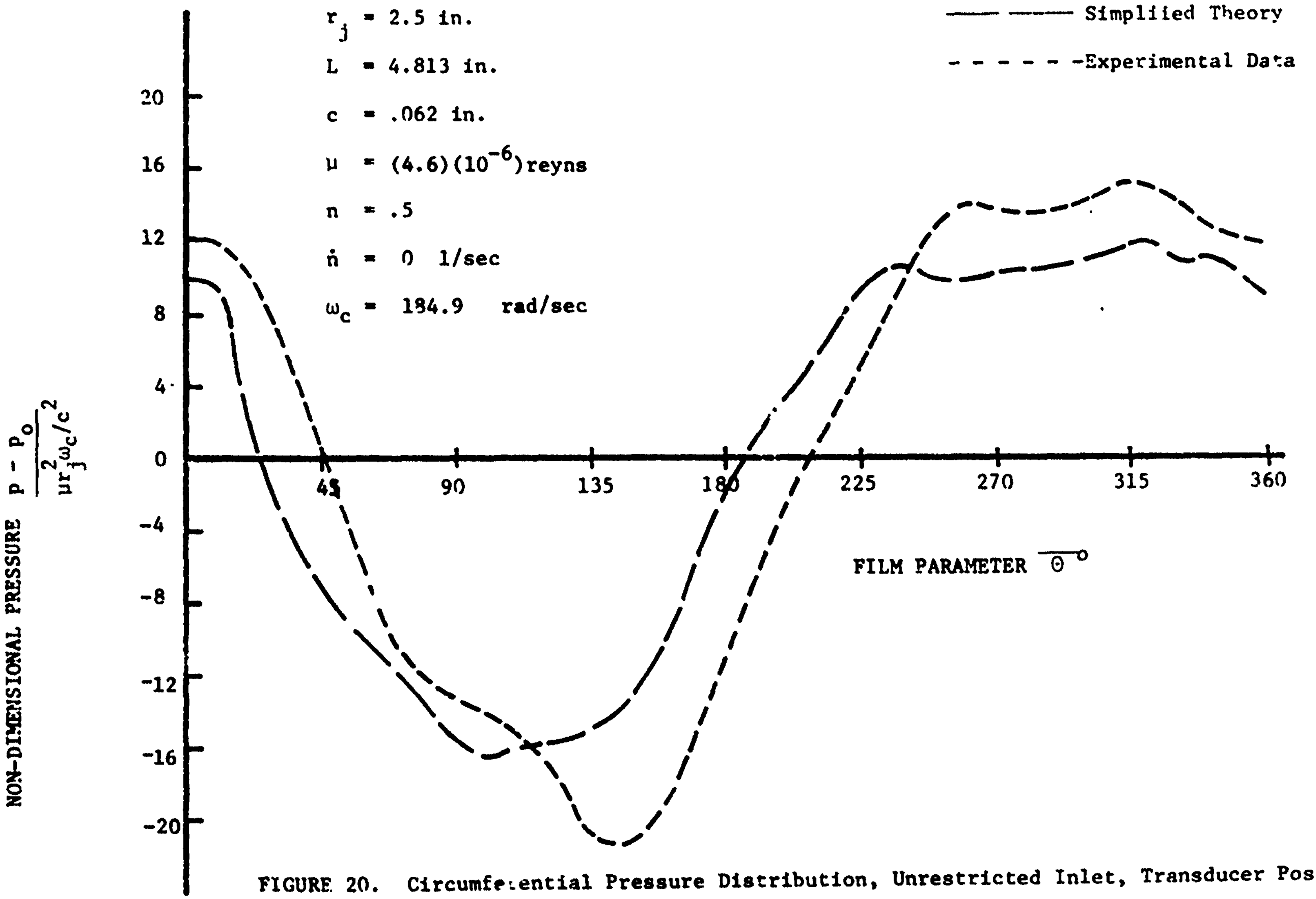

FIGURE 20. Circumferential Pressure Distribution, Unrestricted Inlet, Transducer Position 0°

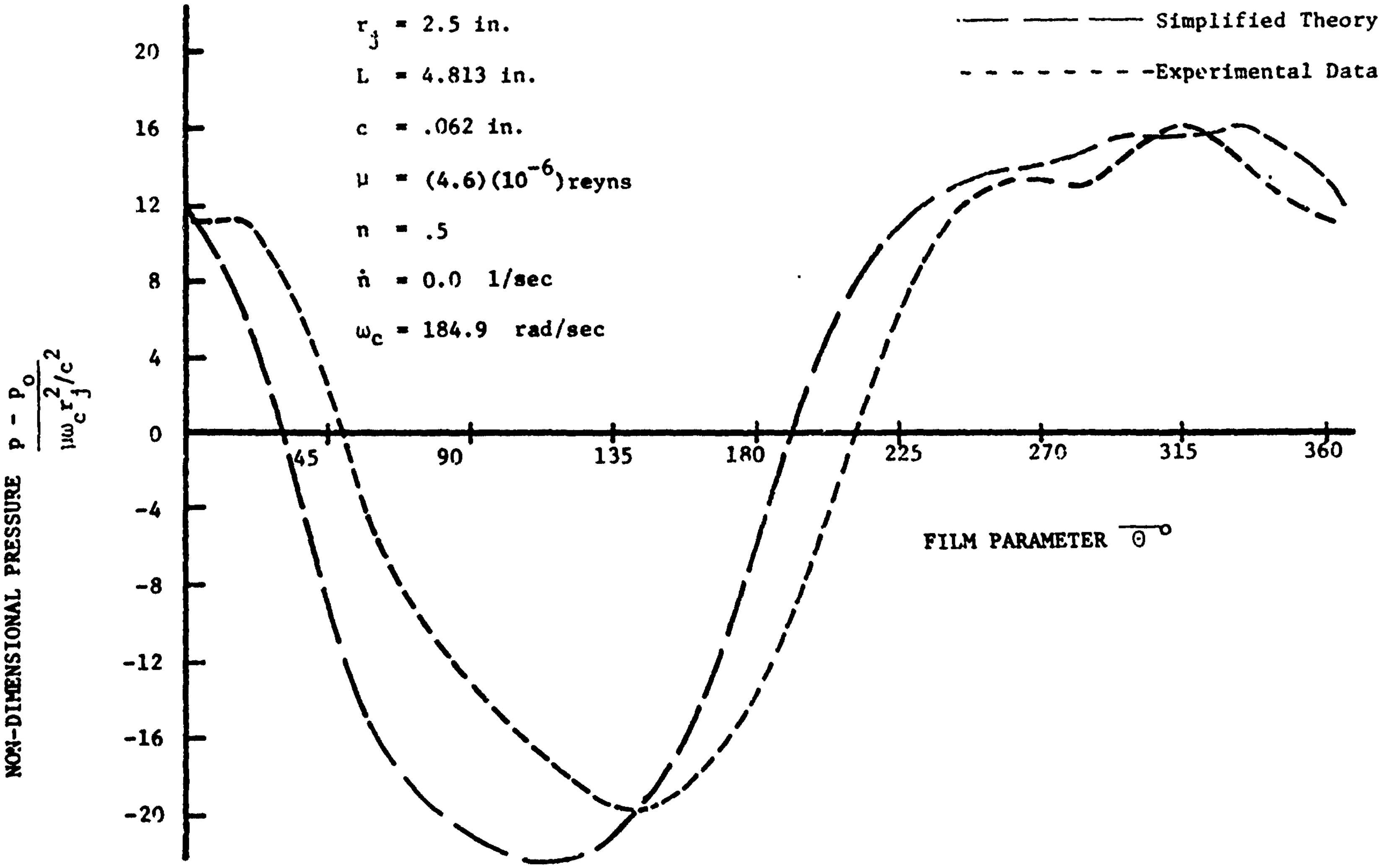

FIGURE 21. Circumferential Pressure Distribution, Unrestricted Inlet, Transducer Position 180°

journal was made to orbit about a point above the center of the outer housing and a known n, $\dot{n}$, and ω_c were obtained as functions of the shaft position. SAE 50 oil was used for these tests.

The pressure distribution around the journal was found by recording the pressure, corresponding to that particular journal location, from each of the photographs for the 36 positions of outer housing. As discussed in the previous section, for the centered orbit case, changes were occurring in the pressure distribution as the outer housing was rotated. The effect of these changes on the accuracy of the data-taking process for the offset orbit case cannot be determined, but may be significant.

As the outer housing was rotated, the pressure distribution, as experienced by the inlet, was constantly changing. Due to this, the value of p_o for each different position of the outer housing, corresponding to each photograph, was different. To correct for this, a specific value of p_o was chosen and each pressure distribution for the 36 positions of the outer cylinder, was adjusted so that each distribution had the same value of p_o.

Data are presented for four perpendicular positions of the eccentric shaft. These positions are 0, 90, 180 and 270 degrees from the vertical up position, in the direction of shaft rotation. The experimental results are shown in Figures 22, 23, 24 and 25 in comparison to the "short bearing" and "long bearing" solutions to Reynolds' equation.

As can be seen from the figures, there is considerable difference between the experimental results and the theory. In Figures 22 and 24 the eccentric shaft is in the vertical up and vertical down position where $\dot{n}$ is zero. Thus, in looking back to the results of the centered orbit case, where $\dot{n}$ is also zero, it would be expected that the experimental results should follow the theory with reasonable agreement, at least to the general shape of the curves.

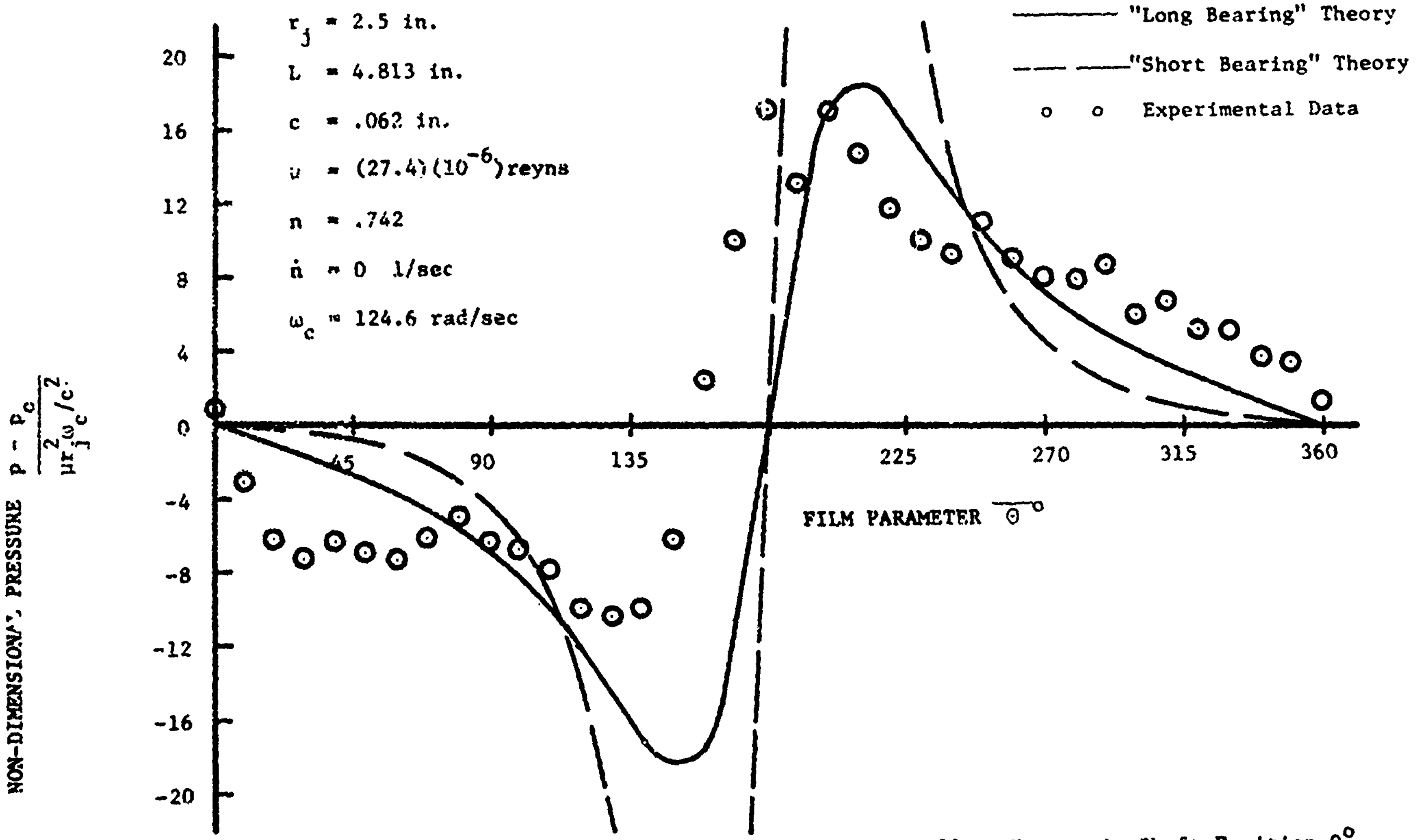

FIGURE 22. Circumferential Pressure Distribution, Offset Eccentric Shaft Position 0°

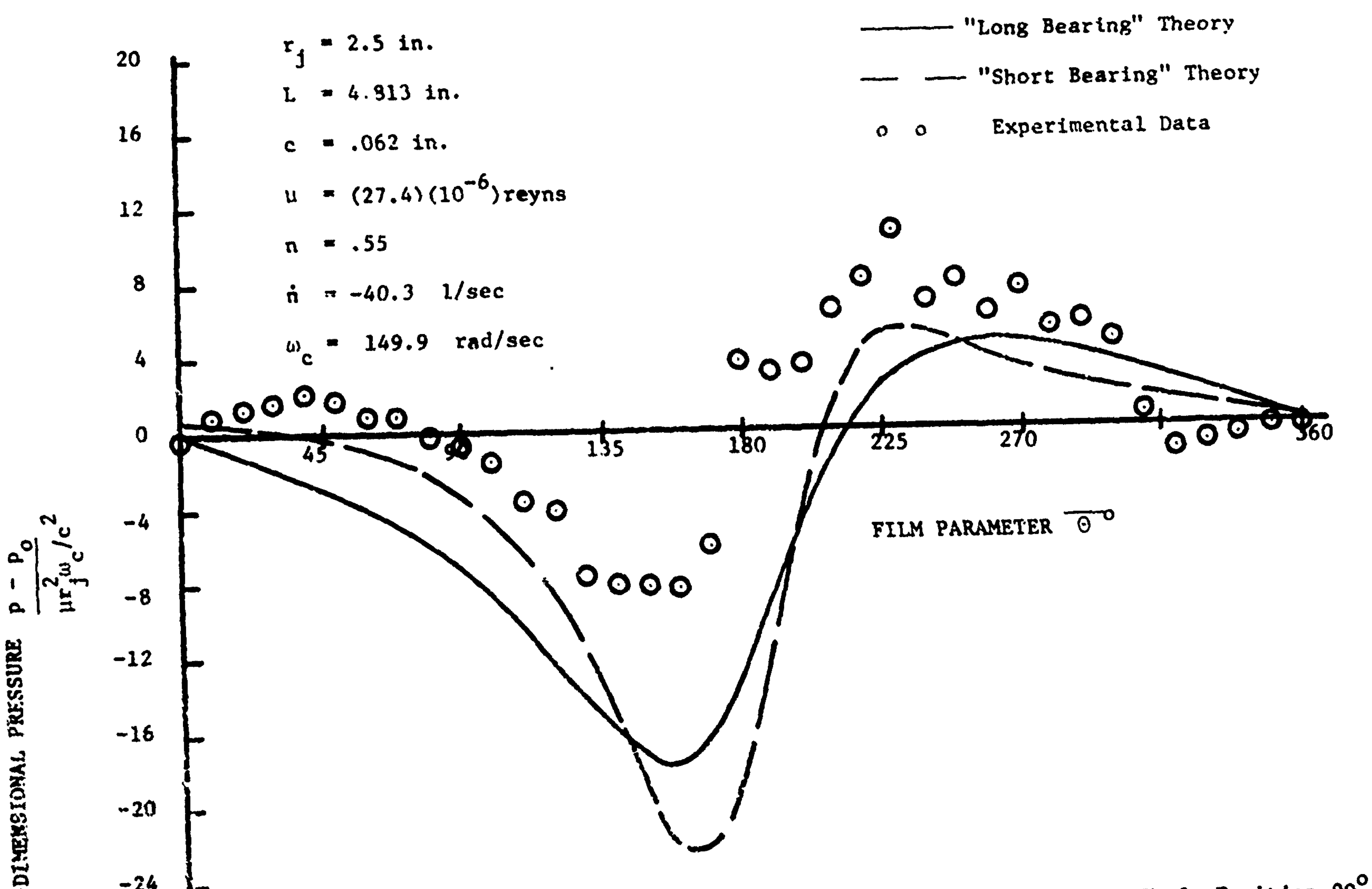

FIGURE 23. Circumferential Pressure Distribution, Offset Eccentric Shaft Position 90°

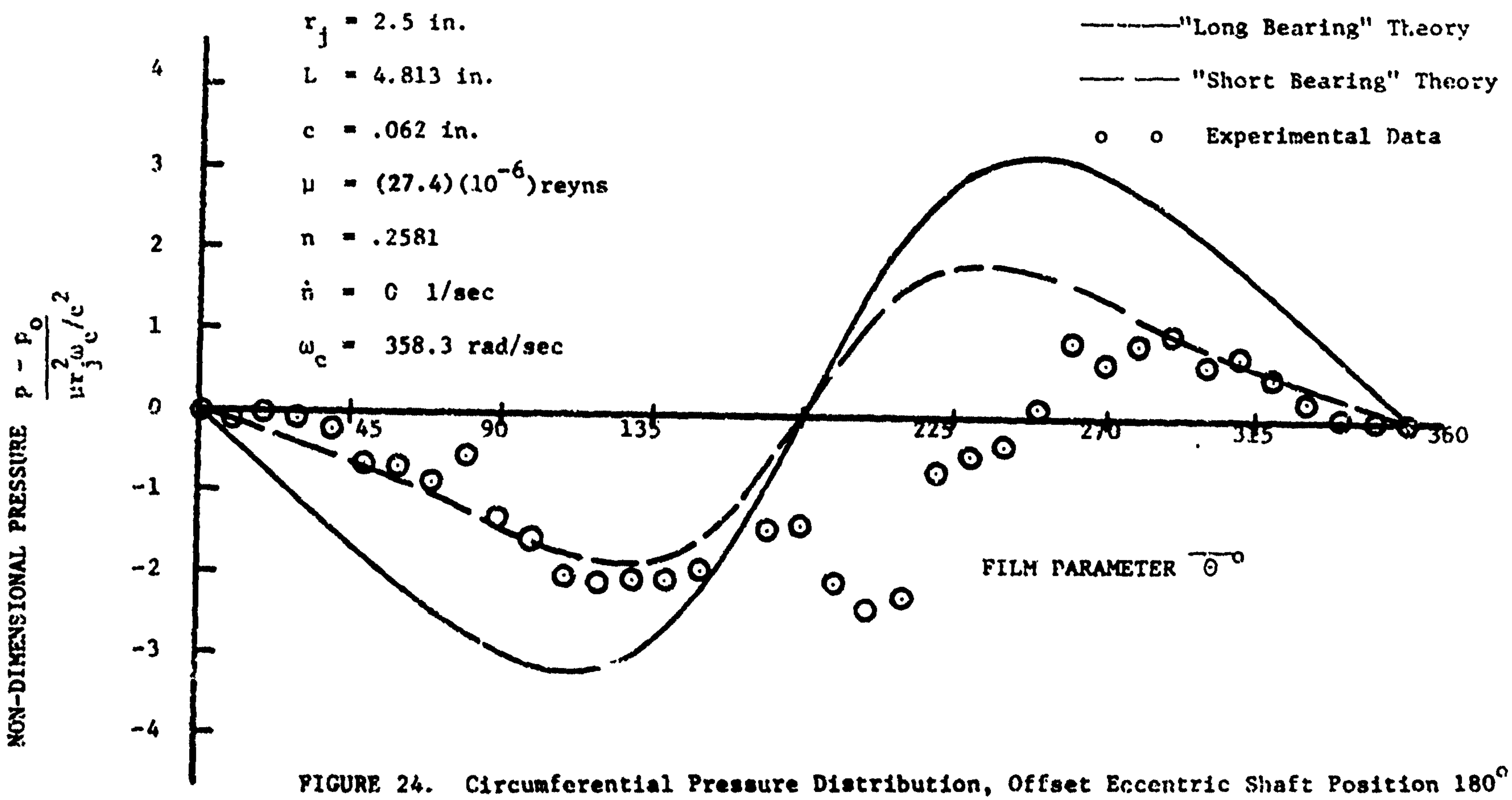

FIGURE 24. Circumferential Pressure Distribution, Offset Eccentric Shaft Position 180°

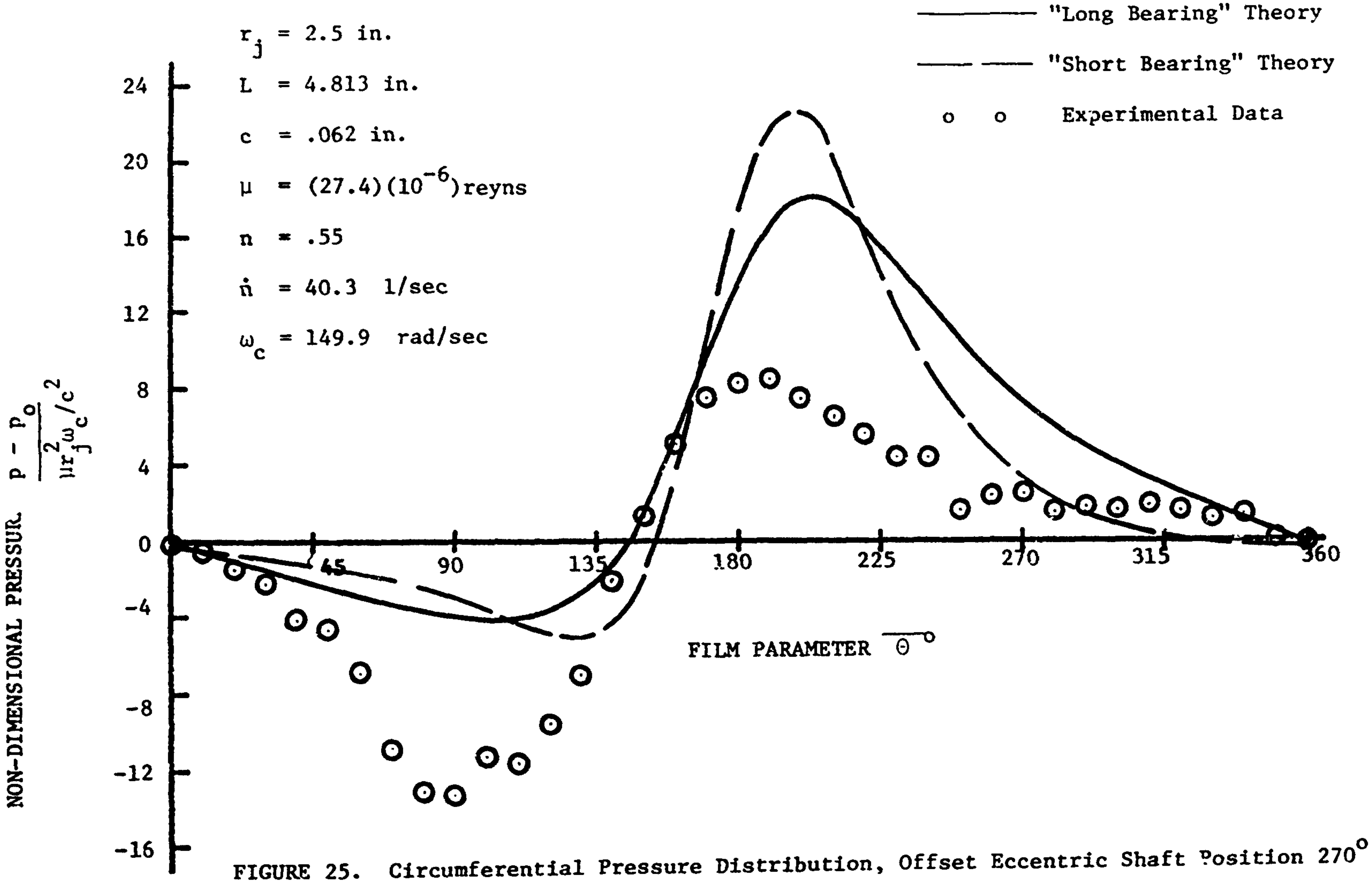

FIGURE 25. Circumferential Pressure Distribution, Offset Eccentric Shaft Position 270°

This is true only for certain portions of the curve as seen . Figure 24. This would indicate that either the measurements are inaccurate or that the fluid flow characteristics are altered because the journal has a non-zero $\dot{n}$ and $\dot{\omega}_c$ over all other portions of its orbit.

The pressure distribution about the journal when located 90 and 270 degrees from the vertical up position are shown in Figures 23 and 25. For these two positions n and ω_c are identical and $\dot{n}$ is of the same magnitude but differs in sign. In both cases the experimental results do not follow the theory. It should be noted that for both cases a reasonably smooth curve can be fitted through the experimental results.

The pressure data was numerically integrated to obtain the radial and tangential force components and the damping coefficient B. The force components, damping coefficient B, and the values predicted using the "long bearing" theory are presented in Table 3. As would be expected there is considerable disagreement between the force components derived experimentally and those predicted by the "long bearing" theory.

As discussed previously, the analytical treatment in current literature of the case of a non-zero $\dot{n}$ is not consistent for either squeeze film dampers or journal bearings. There is also no experimental verification of any theory for the case of a non-zero $\dot{n}$. Thus, the results of this study should not be discourted simply because they do not agree with the existing theories. The large disagreement between these results and the "long bearing" theory may indicate that the "long bearing" theory does not accurately describe the squeeze film for the case of a non-zero $\dot{n}$.

The transition from laminar to vortex or turbulent flow has not been investigated for journal bearings or squeeze film dampers for the case of a non-zero $\dot{n}$. It is possible that some combination of $\dot{n}$, ω_c and n over portions of the journal orbit, for the offset orbit case, result in the formation of

Eccentric Shaft Position	n	$\dot{n}$ (1/sec)	ω_c (rad/sec)	EXPERIMENTAL DATA			"LONG BEARING" THEORY		
				Tangential (lbf)	Radial (lbf)	B (lbf-sec/in	Tangential (lbf)	Radial (lbf)	B (lbf-sec/in)
0°	.742	0.0	124.6	2084.8	811.6	363.7	2238.3	0.0	390.5
90°	.55	40.3	149.9	1160.8	-163.7	224.8	1795.1	-1450.0	347.7
180°	.258	0.0	358.3	520.9	-616.2	90.9	1917.5	0.0	334.5
270°	.55	40.3	149.9	1630.2	687.4	315.8	1795.1	1450.0	347.7

$\mu = (27.4)(10^{-6})$ reyns
$r_j = 2.5$ in.
$L = 4.813$ in.
$c = .062$ in.

$$B = \frac{F_x}{e\omega_c}$$

TABLE 3: FORCE COMPONENTS FOR OFFSET ORBIT CASE

vortex or turbulent flow. This would account for the discrepancies between the "long bearing" theory and the experimental results.

CONCLUSIONS AND RECOMMENDATIONS

Conclusions

The following conclusions were drawn from this study:

1. For a damper with end seals preventing axial flow, the "long bearing" theory is reasonably accurate in predicting the shape of the pressure distribution for the centered orbit case. This holds true for the vortex flow regime as well as for laminar flow. However, the peak to peak magnitude of the pressure distribution is not accurately predicted by this theory, even in the laminar flow regime.
2. The SAE 10 oil produced pressures and resulting force components significantly greater than predicted by the "long bearing" theory. Calculation of the transition parameter presented by Vohr [8] indicates that the damper was operating in the vortex flow regime, resulting in the greater magnitude of the peak to peak pressures. Subsequent calculation of this parameter for actual squeeze film dampers indicates that many dampers may be operating in the vortex or turbulent flow regime.
3. The SAE 50 oil produced pressures and resulting force components significantly less than predicted by the "long bearing" theory. Calculation of the transition parameter indicates that the damper was operating in the laminar flow regime. A possible explanation for the deviation of the experimental results from the "long bearing" theory is the differing boundary conditions of the test rig from the theory due to the use of end seals.
4. A radial inlet with no circumferential grooving results in significant deviation from the "long bearing" theory. An unrestricted radial inlet results in a cyclic variation of the force components of the squeeze film and can result in the loss of the load carrying ability of the film over portions of each cycle.

5. Efficient end seals (minimal end leakage) result in a negligible pressure variation in the axial direction, consistent with the "long bearing" theory.

6. Although the experimental results for the offset orbit case are not sufficiently accurate or complete to form a reliable prediction model, it can be stated with reasonable confidence that the "long bearing" theory does not accurately predict the pressure distribution for this case (cyclic variation of n, $\dot{n}$, and ω_c).

Recommendations for Future Research

It is recommended that several basic modifications ' carried out on the test apparatus to extend the investigation begun in this study. The following is a list of possible modifications:

1. Machine a central circumferential groove in the outer housing to be used as the oil inlet to the squeeze film. This will eliminate the problems inherent with a radial inlet and be more consistent with designs currently being used by several engine manufacturers.
2. Machine the outer housing for additional pressure transducers in the axial direction to determine the axial pressure distribution, which would be more significant with a central circumferential inlet. The addition of several thermocouples can determine if there is a significant axial or circumferential temperature gradient.
3. Replace the o'ring seals, used at the journal ends, with metal piston ring type seals. This will eliminate the possible volumetric change within the squeeze film clearance cause by expansion and contraction of the flexible o'rings.

With the above modifications, the centered orbit case could be studied more thoroughly. Perhaps one of the most interesting areas to be investigated is the relationship between lubricant viscosity and the magnitude of the resulting squeeze film pressures. This study could also lead to an accurate determination of the transition from laminar to vortex or turbulent flow in the case of a rotating line of centers (orbiting damper journal).

A more accurate method of determining the angular position of the eccentric shaft is needed to study the offset orbit case. Data for this case consists of discrete data points, for a particular journal location, taken from each of the pressure distributions obtained from the 36 positions of the outer housing. This requires greater accuracy than was available with the method used in this study. Perhaps high speed strip chart recorders could be used to more accurately record this data.

BIBLIOGRAPHY

1. Cooper, S., "Preliminary Investigation of Oil Films for the Control of Vibration," Institution of Mechanical Engineers (England), Lubrication and Wear Convention. 1963.

2. White, D.C., "The Dynamics of a Rigid Rotor Supported on Squeeze Film Bearings," Conference on Vibrations in Rotating Systems, London, Proceedings, Institution of Mechanical Engineers, Feb. 14-15, 1972.

3. Vance, J. M. and Lee, J., "Stability of high Speed Rotors with Internal Friction," ASME Journal of Engineering for Industry, August 1974, pp. 960-968.

4. Sweet, J. and Genin, J., "Squeeze Film Bearing for the Elimination of Oil Whip," ASME Journal of Lubrication Technology, April 1971, pp. 252-261.

5. Mohan, S. and Hahn, E. J., "Design of Squeeze Film Damper Supports for Rigid Rotors," ASME Journal of Engineering for Industry, August 1974, pp. 976-982.

6. Thomsen, K. K. and Anderson, H., "Experimental Investigation of a Simple Squeeze Film Damper," ASME Paper No. 73-DET-101, ASME Design Engineering Technical Conference, Sept. 9-12, 1973, Cincinnati, Ohio.

7. Jones, M. G., "An Experimental Investigation of Squeeze Film Hydrodynamics," Report No. R. 320, National Gas Turbine Establishment, Ministry of Defence (England), Jan. 1973.

8. Vohr, John, "Experimental Study of the Superlaminar Flow Between Nonconcentric Rotating Cylinders," NASA Contractor Report CR-749, June, 1967.

9. Trumpler, P. R., Design of Film Bearings, Macmillan Company, New York, New York, 1966, pp. 103-163.

10. Dubois, G. B. and Ocvirk, F. W., "Analytical Derivation and Experimental Evaluation of Short-Bearing Approximation for Full Journal Bearings," Report 1157, Nation Advisory Committee for Aeronautics, 1953.

11. Tondl, A., Some Problems of Rotor Dynamics, Chapman and Hall, London, England, 1965, pp. 122-130.

12. Hori, Y., "A Theory of Oil Whip," ASME Journal of Applied Mechanics, June 1959, pp. 189-198.

13. Lund, J. W. and Saibel, E., "Oil Whip Whirl Orbits of a Rotor in Sleeve Bearings, "ASME Journal of Engineering for Industry, Nov. 1967, pp. 813-822.

APPENDIX I

OIL VISCOSITY INFORMATION

Two oils of differing viscosity were used during the experimentation. Viscosity information on the oils was obtained from the manufacturers. The viscosity and related information for the two oils is given below:

SAE 10 Oil

The SAE 10 oil was produced by the Ashland Oil Company (Valvoline). Viscosity information on this oil was obtained from the Product Applications Department:

Temperature	Viscosity
100°F	186.7 SUS
210°F	45.91SUS

These values were plotted on an ASTM (American Society for Testing Materials) Standard Viscosity-Temperature Chart. When the Saybolt Universal Viscosity-Temperature relationship is plotted on the ASTM chart, the resulting curve is a straight line. Consequently if the viscosity temperature relationship is known at two points, i.e. 100°F and 210°F, then all points will fall on the line connecting these points. Thus the viscosity at any temperature can be read from this line. All data using the SAE 10 oil were recorded at an oil temperature of 103°F. The viscosity corresponding to this temperature is 170 SUS.

Using standard unit conversions the viscosity was obtained in reyns:

$$u = (4.6)(10^{-6})\text{reyns} \quad (\text{lb-sec/in}^2)$$

SAE 50 Oil

The SAE 50 oil was produced by the Standard Oil Company. Viscosity information was obtained from them on request:

Temperature	Viscosity
100°F	1650 SUS
210°F	90 SUS

These values were also verified by another researcher at the University of Florida.

Again these values were plotted on an ASTM Standard Viscosity-Temperature Chart. All the data using the SAE 50 oil were recorded at an oil temperature of 115°F. The viscosity corresponding to this temperature is 950 SUS.

Using standard unit conversions the viscosity was obtained in reyns:

$$\mu = (2.74)10^{-5} \text{reyns} \quad (\text{lb-sec/in}^2)$$

APPENDIX II

DIMENSIONS OF SQUEEZE FILM APPARATUS

D_j (diameter of journal)	5.0 in.
r_j (radius of journal)	2.5 in.
L (length of journal)	4.813 in.
Db (inside diameter of outer housing)	5.125 in.
c (clearance $(Db-D_j)/2$)	.062 in.

Centered Orbit Case

n (e/c)	.50
$\dot{n}$ $(\dot{e}/c)$	0.0
ω_c (angular speed of eccentric shaft)	184.9 rad/sec

Offset Orbit Case

A .015 inch shim was placed under eccentric shaft supports. Thus the journal was made to orbit about a point .015 in. above the center of the outer housing. The parameters listed below varied continuously between the given values, as a function of the eccentric shaft position.

n (maximum)	.742
n (minimum)	.258
ω_c (maximum)	358.3 rad/sec
ω_c (minimum)	124.6 rad/sec
$\dot{n}$ (maximum)	44.7 1/sec
$\dot{n}$ (minimum)	-44.7 1/sec

APPENDIX III

PRESSURE TRANSDUCER CALIBRATION INFORMATION

Two Viatran Model 210 strain gage type pressure transducers were used during this study. Calibration data were supplied by the manufacturer but proved to be inaccurate. The transducers were therefore recalibrated using a dead weight tester manufactured by Amthor Testing Instrument Company. The resulting calibration curves are shown in Figures 26 and 27.

The calibration data were also used to derive equations to be used in the computer programs for data analysis. The resulting equations are given below:

Model PTB710G-100 (Serial No. 142571)

Pressure (psig) = 5.5033 x voltage output (mv) + .92

Model PTB210A-200 (Serial No. 288074)

Pressure (psig) = 8.146 x voltage output (mv) - 11.349

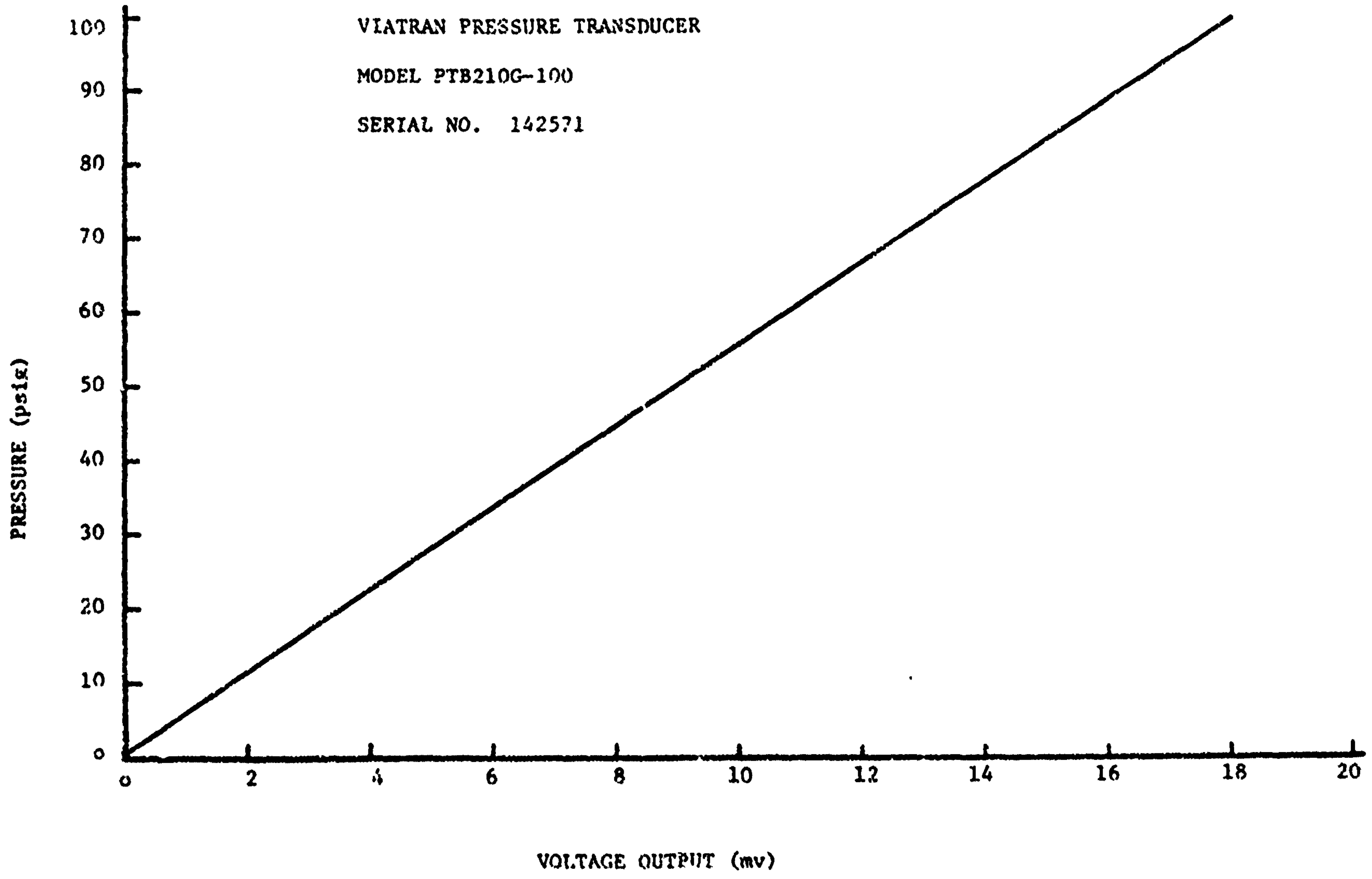

FIGURE 26. Transducer Calibration Curve, 0 - 100 PSIG

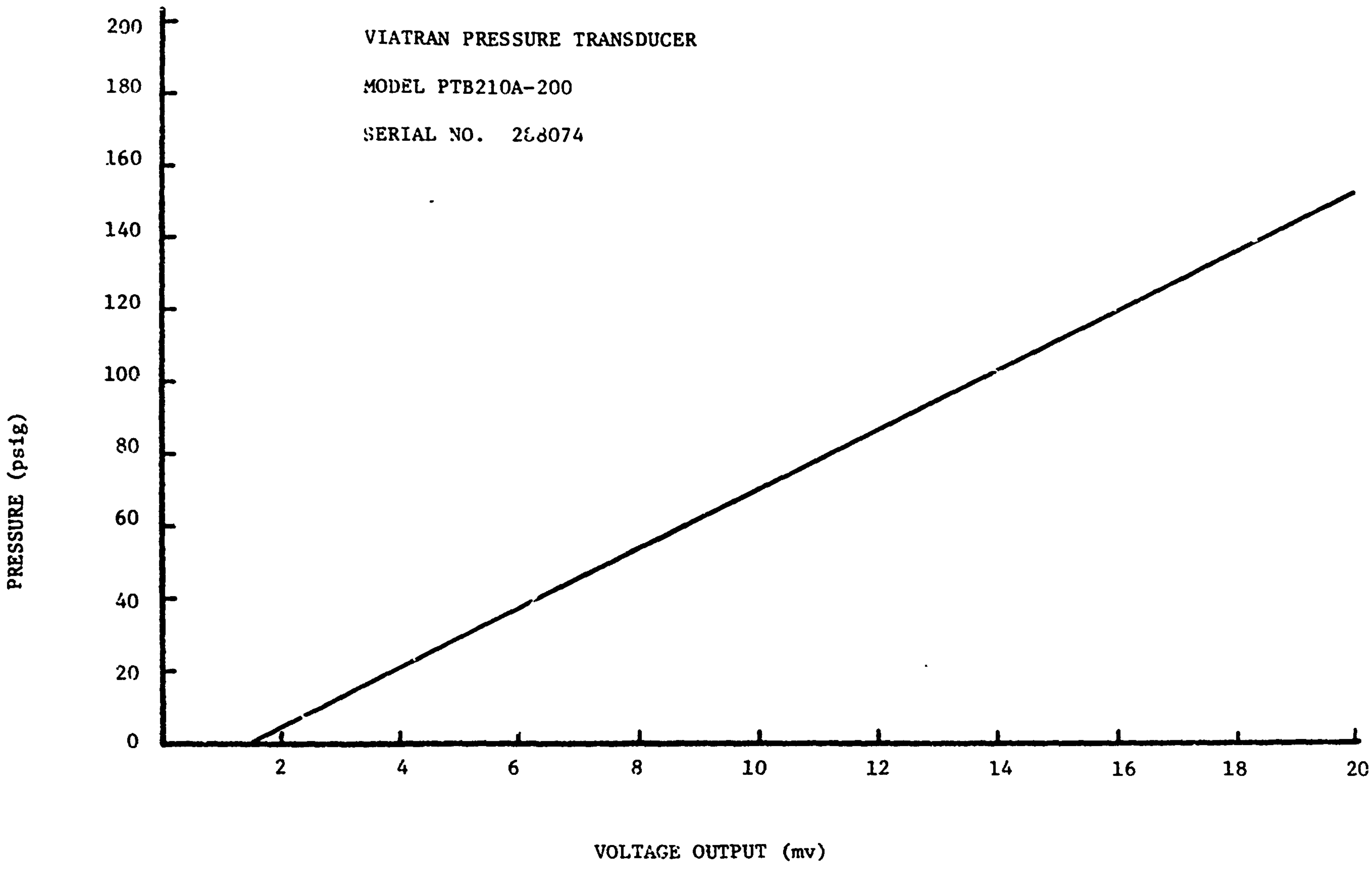

FIGURE 27. Transducer Calibration Curve, 0 - 200 PSIA

APPENDIX IV

DESCRIPTIONS OF COMPUTER PROGRAMS USED IN DATA ANALYSIS

Several computer programs were written in order to analyze the data obtained from this study. The following is a description of each of the programs. Included is a listing of each program.

1. Calculation of the Pressure Distribution Using the "Long Bearing" Theory.

   This program calculates the circumferential pressure distribution about a moving journal using the "long bearing" theory. The journal position, radial velocity, tangential velocity, oil viscosity and other pertinent squeeze film parameters are input. The output is the pressure distribution about the journal as a function of θ, given in ten degree increments.

2. Calculation of the Pressure Distribution Using the "Short Bearing" Theory.

   This program calculates the circumferential pressure distribution about the center of the journal using the "short bearing" theory. The journal position, radial and tangential velocity, oil viscosity, and other pertinent squeeze film parameters are input. The output is the pressure distribution about the center of the journal given in ten degree increments of θ.

3. Calculation of the Pressure Distribution and Force Components From the Experimental Data.

   This program determines the pressure distribution and calculates the radial and tangential force components using the experimental data. The experimental data (output of the pressure transducers in mv.) are input into the program. Using the calibration equations of the transducers (see Appendix III) the pressure distribution about the journal is determined. The pressure distribution is then output in ten degree increments of $\bar{\theta}$. Using the pressure data the integrals for the force components (given below) are numerically integrated using Simpson's Rule:

$$Fx = -Lr_j \int_o^{2\pi} p \sin\theta \, d\theta$$

$$Fy = -Lr_j \int_o^{2\pi} p \cos\theta \, d\theta$$

The radial (F_y) and tangential (F_x) force components are then output from the program.

4. Calculation of the Pertinent Squeeze Film Parameters for the Offset Orbit Case.

This program uses the geometric relationships of the test rig to calculate the values of n , $\dot{n}$, θ , and ω_c as functions of the angular position of the offset eccentric shaft. The input is the dimensions of the test rig and the thickness of the shims used to offset the eccentric shaft. The output is n, $\dot{n}$, ω_c , and the position of the line of centers, as a function of the eccentric shaft position, given in ten degree increments of the shaft rotation. The program then uses the "long bearing" theory to predict the pressures experienced by the pressure transducer as the eccentric shaft rotates. The output is the predicted pressure distribution as experienced by the pressure transducer in ten degree increments of the eccentric shaft position.

5. Calculation of the Four Force Coefficients for the Offset Orbit Case.

This program determines the four force coefficients, as defined by Tondl [9], from the experimental data for two positions of journal. As proposed by Tondl, these force coefficients are functions of n only. For the offset orbit case, there are two positions of the eccentric shaft which result in identical values of n. Thus the force coefficients for these two positions should be identical.

$$\begin{bmatrix} Fx_1 \\ Fy_1 \\ Fx_2 \\ Fy_2 \end{bmatrix} = c \begin{bmatrix} A \end{bmatrix} \begin{bmatrix} F1(n) \\ F2(n) \\ F3(n) \\ F4(n) \end{bmatrix}$$

$$c = 6\pi \mu L r_j^3/c^2$$

$$\begin{bmatrix} A \end{bmatrix} = \begin{bmatrix} 0 & 0 & (-2\omega_c)_1 & (2\dot{n})_1 \\ (-2\omega_c)_1 & (2\dot{n})_1 & 0 & 0 \\ 0 & 0 & (-2\omega_c)_2 & (2\dot{n})_2 \\ (-2\omega_c)_2 & (2\dot{n})_2 & 0 & 0 \end{bmatrix}$$

The subscripts (1) and (2) refer to the two positions of the eccentric shaft with identical n. The force coefficients may then be solved for:

$$\begin{bmatrix} F1(n) \\ F2(n) \\ F3(n) \\ F4(n) \end{bmatrix} = \frac{1}{c} \begin{bmatrix} A \end{bmatrix}^{-1} \begin{bmatrix} F_{x1} \\ F_{y1} \\ F_{x2} \\ F_{y2} \end{bmatrix}$$

The force components, F_{x_1}, F_{y_1}, F_{x_2} and F_{y_2} are determined by numerically integrating the pressure data for the two journal positions. The inverse of matrix A is found using the scientific subroutine MINV. Matrix multiplication is then carried out to deterimine the force coefficients. The shaft position, position of the line of centers, n , $\dot{n}$, ω_c , F_{x_1} , F_{y_1} , F_{x_2} , F_{y_2} and the force coefficients F1(n) , F2(n) , F2(n) and F4(n) are output.

PROGRAM 1

PRESSURE DISTRIBUTION - ''LONG BEARING'' THEORY

```
      C=.062
      WS=184.94
      ED=0.
      E=.5
      I=0
      U=.00002738
      RJ=2.5
      WPR=-2.
      X=6*U*RJ*RJ*WS/(C*C)
      PO=50./X
      WRITE (6,4)
    4 FORMAT ('1'.////////,T22,'THETA',T33,'PRESSURE',T46,
     1'NONDIM. PRESS.')
    2 IF (I.GT.360) GO TO 1
      TH=I/57.295779
      Z=(1+E*COS(TH))**2
      P=X*(PO+(WPR*E*SIN(TH)*(2+E*COS(TH)))/((2+E*E)*Z)+(ED/(2*E)
     1)*((1/Z)-(1/(1+E)**2))*2/WS)
      DPJ=(P-PO*X)*6./X
      TH=TH*57.295779
      WRITE (6,5) I,P,DPJ
    5 FORMAT (I25,2F15.4)
      I=I+10
      GO TO 2
    1 CONTINUE
      WRITE (6,18)
   18 FORMAT ('1')
      STOP
      END
```

```
$DATA
```

Reproduced from
best available copy.

PROGRAM 2

PRESSURE DISTRIBUTION - ''SHORT BEARING'' THEORY

```
      U=.00002738
      E=.5
      ED=0.
      WS=184.94
      PO=50.
      EL=4.813
      C=.062
      I=0
      X3=0.
      RJ=2.5
      WRITE (6,2)
    2 FORMAT ('1',/////////,T22,'THETA',T33,'PRESSURE',T46,
     1'NONDIM. PRESS.')
    1 IF (I.GT.360) GO TO 3
      TH=I/57.295779
      Z=1+E*COS(TH)
      P=PO+6*U*(ED*COS(TH)+WS*E*SIN(TH))*(X3*X3-EL*EL/4.)/(C*C*(Z*
     1*3))
      DP=(P-PO)*C*C/(U*WS*RJ*RJ)
      WRITE (6,4)I,P,DP
    4 FORMAT (I25,2F15.4)
      I=I+10
      GO TO 1
    3 CONTINUE
      WRITE (6,18)
   18 FORMAT ('1')
      STOP
      END
$DATA
```

Reproduced from best available copy.

PROGRAM 3

PRESSURE DIST. AND FORCE COMPONENTS - EXPERIMENTAL DATA

```
      DIMENSION P(37),PX(37),PY(37)
      DATA P/8.,7.64,7.3,6.92,6.4,5.82,5.26,4.66,4.2,4.,3.6,3.3,2
     1.94,2.52,2.4,2.6,3.34,4.76,6.78,8.8,10.2,11.3,12.4,12.6,12.
     16,12.4,11.86,11.3,10.84,10.54,10.2,10.,9.6,9.2,8.8,8.4,8./
      PO=50.
      RJ=2.5
      U=.00002738
      WS=184.94
      C=.062
      K=0
      H=10/57.295779
      TH=0.
      PTTX=0
      PTTY=0
      I=1
      J=1
      WRITE (6,12)
   12 FORMAT ('1',////////,T22,'THETA',T33,'PRESSURE',T46,
     1'NONDIM. PRESS.')
    9 IF (J.GT.37) GO TO 10
      P(J)=8.146*P(J)-11.349
      DP=(P(J)-PO)*C*C/(U*WS*RJ*RJ)
      WRITE (6,11) K,P(J),DP
   11 FORMAT (I25,2F15.4)
      K=K+10
      J=J+1
      GO TO 9
   10 CONTINUE
    8 IF (I.GT.37) GO TO 7
      PX(I)=P(I)*SIN(TH)
      PY(I)=P(I)*COS(TH)
      I=I+1
      TH=TH+H
      GO TO 8
    7 CONTINUE
      I=1
    2 IF (I.GT.36) GO TO 1
      PTX=(PX(I)+4*PX(I+1)+PX(I+2))*H/3
      PTY=(PY(I)+4*PY(I+1)+PY(I+2))*H/3
      PTTX=PTTX+PTX
      PTTY=PTTY+PTY
      I=I+2
      GO TO 2
    1 CONTINUE
      FX=-4.813*2.5*PTTX
      FY=-4.813*2.5*PTTY
      WRITE (6,6)
    6 FORMAT (///,T32,'F(X)',T47,'F(Y)')
      WRITE (6,5) FX,FY
    5 FORMAT (1F36.4,1F15.4)
      WRITE (6,18)
   18 FORMAT ('1')
      STOP
      END

$DATA
```

PROGRAM 4

SQUEEZE FILM PARAMETERS FOR OFFSET ORBIT CASE

```
      DIMENSION EN(37),END(37),WCC(37),THE(37)
      I=0
      S=.015
      WS=184.94
      EP=.031
      GA=0.0
      C=.062
      J=1
      THO=20.
      U=.0000273B
      RJ=2.5
      X=6*U*RJ*RJ*WS/(C*C)
      P0=40/X
      WRITE (6,2)
    2 FORMAT ('1',/////////,T18,'SHAFT ANGLE',T36,'N',T48,'N-DOT',
     1T52,'THETA',T74,'W-C')
    3 IF (I.GT.180) GO TO 5
      E=SQRT(S*S+2*S*EP*COS(GA)+EP*EP)
      ED=-(S*EP*SIN(GA)*WS/E)
      IF (I.EQ.0) GO TO 6
      IF (I.EQ.180) GO TO 7
      Z=((S*S)+(E*E)-(EP*EP))/(2.*S*E)
      TH=ARCOS(Z)
      WC=-((ED/S)-(Z*ED/E))/SQRT(1.-(Z*Z))
      GO TO 9
    6 TH=0.0
      GO TO 8
    7 TH=180/57.2958
    8 WC=EP*WS/E
    9 CONTINUE
      K=38-J
      EN(J)=E/C
      EN(K)=EN(J)
      END(J)=ED/C
      END(K)=-END(J)
      WCC(J)=WC
      WCC(K)=WC
      THE(J)=TH*57.295779
      THE(K)=360.-THE(J)
      J=J+1
      I=I+10
      GA=I/57.295779
      GO TO 3
    5 CONTINUE
      GA=0.0
      J=1
   10 IF (J.GT.37) GO TO 11
      WRITE (6,12) GA,EN(J),END(J),THE(J),WCC(J)
   12 FORMAT (1F25.1,2F14.3,1F12.1,1F13.2)
      J=J+1
      GA=GA+10
      GO TO 10
   11 CONTINUE
      GA=0.0
      I=0
      J=1
      WRITE (6,13)
   13 FORMAT ('1',/////////,T18,'SHAFT ANGLE',T36,'THETA',T50,
     1'PRESSURE')
   14 IF (I.GT.360) GO TO 15
      TH=THO+180-THE(J)
      IF (TH.GT.0) GO TO 16
      TH=360+TH
   16 CONTINUE
      TH=TH/57.295779
      E=EN(J)
      END(J)=END(J)*2/WCC(J)
      WPR=-(2*WCC(J)/WS)
      Z=(1+EN(J)*COS(TH))**2
      P=X*(P0+(WPR*E*SIN(TH)*(2+EN(J)*COS(TH)))/((2+EN(J)*EN(J))*
     1Z)+(END(J)/(2*EN(J)))*((1/Z)-(1/(1+EN(J))**2))*(2/WS))
      TH=TH*57.295779
      WRITE(6,17) GA,TH,P
   17 FORMAT (1F25.1,2F15.1)
      I=I+10
      GA=GA+10
      J=J+1
      GO TO 14
   15 CONTINUE
      WRITE (6,18)
   18 FORMAT ('1')
      STOP
      END

$DATA
```

PROGRAM 5

FORCE COEFFICIENTS - EXPERIMENTAL DATA, OFFSET ORBIT CASE

```
      DIMENSION A(4,4),END(2),FN(4),FX(2),FY(2),L(4),M(4)
      RJ=2.5
      C=.002
      EL=4.313
      S=.015
      WS=184.94
      EP=.031
      U=.00002738
      X=6*U*EL*(RJ**3)/(C*C)
      GA=60/57.29579
      E=SQRT(S*S+2*S*EP*COS(GA)+EP*EP)
      EN=E/C
      ED=-(S*EP*SIN(GA)*WS)/E
      END(1)=ED/C
      END(2)=-END(1)
      Z=(S*S+E*E-EP*EP)/(2*S*E)
      PHI=ARCOS(Z)
      WC=-(ED/S-Z*ED/E)/SQRT(1-Z*Z)
      WRITE (6,15)
   15 FORMAT ('1',/////////,T20,'N',T31,'N-DOT(1)',T46,'N-DOT(2)',
     1T61,'W-C')
      WRITE (6,16) EN,END(1),END(2),WC
   16 FORMAT (1F22.3,3F15.3)
      A(1,1)=0.
      A(1,2)=0.
      A(1,3)=-2*WC
      A(1,4)=2*END(1)
      A(2,1)=-2*WC
      A(2,2)=2*END(1)
      A(2,3)=0.
      A(2,4)=0.
      A(3,1)=0.
      A(3,2)=0.
      A(3,3)=-2*WC
      A(3,4)=2*END(2)
      A(4,1)=-2*WC
      A(4,2)=2*END(2)
      A(4,3)=0.
      A(4,4)=0.
      N=4
      CALL FORCES (FX,FY)
      CALL MINV(A,N,D,L,M)
      J=1
   11 IF (J.GT.4) GO TO 10
      FN(J)=(A(J,1)*FX(1)+A(J,2)*FY(1)+A(J,3)*FX(2)+A(J,4)*FY(2))/X
      J=J+1
      GO TO 11
   10 CONTINUE
      WRITE (6,13)
   13 FORMAT ('0',///,T20,'FN(1)',T35,'FN(2)',T50,'FN(3)',T65,
     1'FN(4)')
      WRITE (6,12) FN(1),FN(2),FN(3),FN(4)
   12 FORMAT (1F24.3,3F15.3)
      WRITE (6,20)
   20 FORMAT ('1')
      STOP
      END
```

Reproduced from best available copy.

```
      SUBROUTINE FORCES (FX,FY)
      DIMENSION FX(2),FY(2),P(37),PX(37),PY(37),Q(37)
      DATA P/1.96,2.17,2.22,2.27,2.36,2.30,2.15,2.13,1.96,1.87,1.
     17,.1.58,1.32,.75,.55,.64,.62,.97,2.[illegible],2.[illegible],2.55,3.03,3.3,3.7,
     13.1,3.28,[illegible],2.86,2.9,2.75,2.1,1.77,1.83,1.88,1.96,1.95/
      DATA Q/1.93,1.85,1.72,1.6,1.3,1.2,.85,.2,-.15,-.2,.13,.03,.
     141,.83,1.62,2.22,2.31,3.22,3.34,3.37,3.2,3.07,2.9,2.69,2.69,
     12.2,2.35,2.33,2.22,2.27,2.25,2.27,2.22,2.17,2.2,2.2,2.97,1.97/
      K=1
      H=57.295779
   11 CONTINUE
      J=1
      IF (K-2) 9,14,12
    9 CONTINUE
      IF (J.GT.37) GO TO 13
      P(J)=5.*8.14*P(J)-11.349
      J=J+1
      GO TO 9
   14 CONTINUE
      IF (J.GT.37) GO TO 13
      P(J)=5.*8.14*Q(J)-11.349
      J=J+1
      GO TO 14
   13 CONTINUE
      G=0.
      I=1
    8 IF (I.GT.37) GO TO 7
      PX(I)=P(I)*SIN(G)
      PY(I)=P(I)*COS(G)
      I=I+1
      G=G+H
      GO TO 8
    7 CONTINUE
      I=1
      PTTX=0.
      PTTY=0.
    2 IF (I.GT.36) GO TO 1
      PTX=(PX(I)+4.*PX(I+1)+PX(I+2))*H/3.
      PTY=(PY(I)+4.*PY(I+1)+PY(I+2))*H/3.
      PTTX=PTTX+PTX
      PTTY=PTTY+PTY
      I=I+2
      GO TO 2
    1 CONTINUE
      FX(K)=PTTX
      FY(K)=PTTY
      WRITE (6,6)
    6 FORMAT ('0',///,T20,'FX',T35,'FY')
      WRITE (6,5) PTTX,PTTY
    5 FORMAT (1F20.3,1F13.3)
      K=K+1
      GO TO 11
   12 CONTINUE
      RETURN
      END
```

Reproduced from
best available copy.

```
      SUBROUTINE MINV(A,N,D,L,M)
      DIMENSION A(16),L(4),M(4)
      D=1.0
      NK=-N
      DO 80 K=1,N
      NK=NK+N
      L(K)=K
      M(K)=K
      KK=NK+K
      BIGA=A(KK)
      DO 20 J=K,N
      IZ=N*(J-1)
      DO 20 I=K,N
      IJ=IZ+I
   10 IF( ABS(BIGA)- ABS(A(IJ))) 15,20,20
   15 BIGA=A(IJ)
      L(K)=I
      M(K)=J
   20 CONTINUE
      J=L(K)
      IF (J-K) 35,35,25
   25 KI=K-N
      DO 30 I=1,N
      KI=KI+N
      HOLD=-A(KI)
      JI=KI-K+J
      A(KI)=A(JI)
   30 A(JI) =HOLD
   35 I=M(K)
      IF(I-K) 45,45,38
   38 JP=N*(I-1)
      DO 40 J=1,N
      JK=NK+J
      JI=JP+J
      HOLD=-A(JK)
      A(JK)=A(JI)
   40 A(JI) =HOLD
   45 IF(BIGA) 48,46,48
   46 D=0.0
      RETURN
   48 DO 55 I=1,N
      IF(I-K) 50,55,50
   50 IK=NK+I
      A(IK)=A(IK)/(-BIGA)
   55 CONTINUE
      DO 65 I=1,N
      IK=NK+I
      HOLD=A(IK)
      IJ=I-N
      DO 65 J=1,N
      IJ=IJ+N
      IF(I-K) 60,65,60
   60 IF(J-K) 62,65,62
   62 KJ=IJ-I+K
      A(IJ)=HOLD*A(KJ)+A(IJ)
   65 CONTINUE
      KJ=K-N
      DO 75 J=1,N
      KJ=KJ+N
      IF(J-K) 70,75,70
   70 A(KJ)=A(KJ)/BIGA
   75 CONTINUE
      D=D*BIGA
      A(KK)=1.0/BIGA
   80 CONTINUE
      K=N
  100 K=(K-1)
      IF (K) 150,150,105
  105 I=L(K)
      IF(I-K) 120,120,108
```

Reproduced from
best available copy.

```
108   JQ=N*(K-1)
      JR=N*(I-1)
      DO 110 J=1,N
      JK=JQ+J
      HOLD=A(JK)
      JI=JR+J
      A(JK)=-A(JI)
110   A(JI) =HOLD
120   J=M(K)
      IF (J-K) 100,100,125
125   KI=K-N
      DO 130 I=1,N
      KI=KI+N
      HOLD=A(KI)
      JI=KI-K+J
      A(KI)=-A(JI)
130   A(JI) =HOLD
      GO TO 100
150   RETURN
      END
```

Reproduced from
best available copy.

END